Universität Hamburg
DER FORSCHUNG | DER LEHRE | DER BILDUNG

UPPSALA
UNIVERSITET

Master thesis

Superconducting Phase Stiffness and Coherence Length From a Finite Momentum Pairing Constraint

Hamburg, April 2025

Tjark Sievers (7147558)
Department of Physics
First reviewer: Prof. Dr. Tim Wehling
Second reviewer: Prof. Dr. Annica Black-Schaffer (Uppsala University)

Even Einstein [...] had attempted to construct a theory of superconductivity. Fortunately, I was unaware of these many unsuccessful attempts. So when John invited me to join him (he, somehow, neglected to mention these previous efforts), I decided to take the plunge.

Leon Cooper
"Remembrance of Superconductivity Past", BCS: 50 Years [1].

Typeset with LaTeX in TeX Gyre Pagella, TeX Gyre Heros, and `TeX Gyre Cursor`.

Abstract

This thesis investigates superconductivity, with a particular focus on the coherence length (describing the size of Cooper pairs) and the London penetration depth (describing the distance magnetic fields can penetrate into the material). These length scales are connected to the properties of the material when in the superconducting state.

The method is based on the Ginzburg-Landau theory, introducing a finite momentum to the order parameter. To compute these length scales within microscopic theories, this finite momentum must be incorporated into the respective theoretical framework. In the theoretical introduction, this approach is demonstrated for both mean-field Bardeen-Cooper-Schrieffer (BCS) theory and Dynamical Mean Field Theory (DMFT).

A class of systems attracting significant recent interest are those with flat electronic bands, especially Graphene based system that host flat band due to specific structural configurations. One proposed system that is treated in this thesis consists of a layer of group-IV atoms between a Graphene sheet and a SiC substrate. A minimal model for this system is Graphene with one additional atom in the unit cell providing the flat band.

The finite-momentum pairing method is applied to both this decorated Graphene model and a one-band Hubbard model with a simple local attractive interaction. The superconducting length scales are calculated and compared between the BCS and DMFT frameworks.

The thesis concludes with a discussion of the potential applications of this method to more realistic versions of the decorated graphene model and outlines the prospects of a full DMFT treatment in such contexts.

Kurzzusammenfassung

Diese Arbeit untersucht Supraleitung mit einem besonderen Fokus auf die Kohärenzlänge (die die Ausdehnung von Cooper-Paaren beschreibt) und die London'sche Eindringtiefe (die angibt, wie weit Magnetfelder in ein Material eindringen können). Diese Längenskalen sind eng mit den Materialeigenschaften im supraleitenden Zustand verknüpft.

Die Methode basiert auf der Ginzburg-Landau-Theorie, wobei dem Ordnungsparameter ein endlicher Impuls zugewiesen wird. Um diese Längenskalen in mikroskopischen Theorien zu berechnen, muss dieser endliche Impuls in das jeweilige theoretische Rahmenwerk eingeführt werden. In der theoretischen Einleitung wird dieser Zugang sowohl in Bardeen-Cooper-Schrieffer (BCS)-Theorie als auch in Dynamische Molekularfeld-Theorie demonstriert.

Ein Systemtyp, der in jüngerer Zeit verstärktes Interesse auf sich zieht sind solche mit flachen elektronischen Bändern, insbesondere Graphen-basierte Systeme, in denen flache Bänder aufgrund spezieller struktureller Eigenschaften auftreten. Ein in dieser Arbeit behandeltes Beispiel besteht aus einer Schicht von Gruppe-IV-Atomen zwischen einer Graphenlage und einem SiC-Substrat. Ein Minimalmodell für dieses System ist eine modifizierte Graphenstruktur mit einem zusätzlichen Atom in der Einheitszelle, das das flache Band stellt.

Die Methode der Paarbildung mit endlichem Impuls wird sowohl auf dieses dekorierte Graphenmodell als auch auf ein Ein-Band-Hubbard-Modell mit einer einfachen lokalen attraktiven Wechselwirkung angewendet. Die supraleitenden Längenskalen werden berechnet und zwischen den BCS- und DMFT-Ansätzen verglichen.

Die Arbeit schließt mit einer Diskussion über mögliche Anwendungen der Methode auf realistischere Versionen des dekorierten Graphenmodells sowie über die Perspektiven einer vollständigen DMFT-Behandlung in diesem Kontext.

Contents

1 Introduction

2 Superconductivity

Superconductivity research has been pushing our understanding of quantum and material science [2]. In this chapter I will review the concepts necessary for understanding superconductivity and introduce the tools used to study it in the later chapters. There are many textbooks covering these topics which can be referenced for a more detailed treatment, such as refs. [3–7].

The superconducting state is a condensation of electrons into pairs with a macroscopically coherent phase, which spontaneously breaks the $U(1)$ phase rotation symmetry. This fixed phase leads to superfluidity in neutral atoms like H_4 or cold atomic gases and superconductivity in superconductors, which can both be phenomenologically explained in Ginzburg-Landau theory, discussed in section 2.1. Both phenomena are characterized by dissipationless flow, of neutral atoms in one case and charged electron pairs in the other. For this reason, similar nomenclature is used, for example the current in a superconductor is often called a charged superflow.

Ginzburg-Landau theory introduces two length scales inherent to superconductors: the coherence length ξ_0 describing the length scale of amplitude variations of the order parameter and the London penetration depth λ_L, which is connected to energy cost of phase variations of the order parameter. They also connect to the energy gap Δ and the condensate stiffness D_S, which are often competing energy scales in superconductors.

The interplay of these length (energy) scales determine the macroscopic properties of a superconductors, so there is a great interest in accessing them from microscopic theories. To this end, section 2.1 also introduces a theoretical framework based on Cooper pairs with finite momentum [8] that will be used in later chapters to calculate these length scales from microscopic theories. Two of these microscopic theories, BCS (Bardeen-Cooper-Schrieffer) theory and DMFT (Dynamical Mean Field Theory) will be introduced in section 2.2 and section 2.3 respectively.

Furthermore, section 2.4 introduces an emerging perspective in the study of novel superconductors: it turns out that the superfluid weight is connected to a property of the electronic band structure called the quantum metric [9, 10].

2.1 Ginzburg-Landau Theory of Superconductivity

Spontaneous Symmetry Breaking and Order Parameter

Symmetries are a powerful concept in physics. Noethers theorem [11] connects the symmetries of physical theories to associated conservation laws. An interesting facet of symmetries in physical theories is the fact that a ground state of a system must not necessarily obey the same symmetries of its Hamiltonian. So for a symmetry operation that is described by a unitary operator U, the Hamiltonian commutes with U, which results in expectation values of the Hamiltonian being invariant under the symmetry operation, but the states $|\phi\rangle$ and $U|\phi\rangle$ can be different. This phenomenon is called spontaneous symmetry breaking and the state $|\phi\rangle$ is said to be symmetry-broken.

One consequence of this fact is that for a given symmetry-broken state $|\phi\rangle$, there exist multiple states with the same energy that can be reached by repeatedly applying U to $|\phi\rangle$. To differentiate the symmetry-broken states an operator can be defined that has all these equivalent states as eigenvectors with different eigenvalues and zero expectation value for symmetric states. This is the microscopic notion of an order parameter.

The original notion of an order parameter was motivated from macroscopic observables that can then be related to the microscopic order parameter operator introduced above. Macroscopically one characterizes the symmetry breaking by an order parameter Ψ which generally can be a complex-valued vector that becomes non-zero below the transition temperature T_C

$$|\Psi| = \begin{cases} 0 & T \geq T_C \\ |\Psi_0| > 0 & T < T_C \end{cases} . \tag{2.1}$$

In the example of a ferromagnet, a finite magnetization of a material is associated with a finite expectation value for the z-component of the spin operator, $m_z = \langle \hat{S}_z \rangle$ [12]. Similarly to a magnetically ordered state, the superconducting state is characterized by an order parameter. The theory of phase transitions in superconductors was developed by Ginzburg and Landau [13]. Landau theory and conversely Ginzburg-Landau theory is not concerned with the the microscopic properties of the order parameter, but describes the changes in thermodynamic properties of matter when the order parameter assumes a finite value. In the context of superconductivity, the order parameter is a complex

quantity

$$\Psi = \Psi_1 + \mathrm{i}\Psi_2 = |\Psi| e^{\mathrm{i}\phi} \,. \tag{2.2}$$

and is connected to the pairing amplitude

$$\Delta_{\mathbf{k}} = -\sum_{\mathbf{k}'} V_{\mathbf{k},\mathbf{k}'} \langle c_{-\mathbf{k}'\downarrow} c_{\mathbf{k}'\uparrow} \rangle \ , \tag{2.3}$$

i.e. the expectation value for the coherent creation of electron pairs of opposite momentum and spin.

Landau and Ginzburg-Landau Theory

Underlying Landau theory is the concept of the free energy: it is a thermodynamic potential as a function of state variables that is minimized in thermodynamic equilibrium. The fundamental idea of Landau theory is now to write the free energy $F[\Psi]$ as function of the order parameter Ψ and expand it as a polynomial:

$$F_{\mathrm{L}}[\Psi] = \int \mathrm{d}^d x f_{\mathrm{L}}[\Psi] \,, \tag{2.4}$$

where

$$f_{\mathrm{L}}[\Psi] = \frac{r}{2}\Psi^2 + \frac{u}{4}\Psi^4 \tag{2.5}$$

is called the free energy density. The stationary point of f_{L} can be found from the condition

$$\frac{\delta f_{\mathrm{L}}}{\delta \Psi} = r\Psi + u\Psi^3 \stackrel{!}{=} 0 \tag{2.6}$$

which gives

$$\Psi = 0 \ \vee \ \Psi = \pm\sqrt{\frac{r}{u}} \tag{2.7}$$

For a stable systems $r > 0$ is required, so for the order parameter to assume a finite value at a critical temperature T_{C}, the parameter r needs to change sign:

$$r = a(T - T_{\mathrm{C}}) \,. \tag{2.8}$$

Figure 2.1a shows the free energy as a function of a single-component, real order parameter Ψ. When the order parameter can be calculated from a microscopic theory, the critical temperature T_{C} can be extracted from the behavior of the order parameter near T_C via a linear fit of

$$|\Psi|^2 \propto T_C - T \,. \tag{2.9}$$

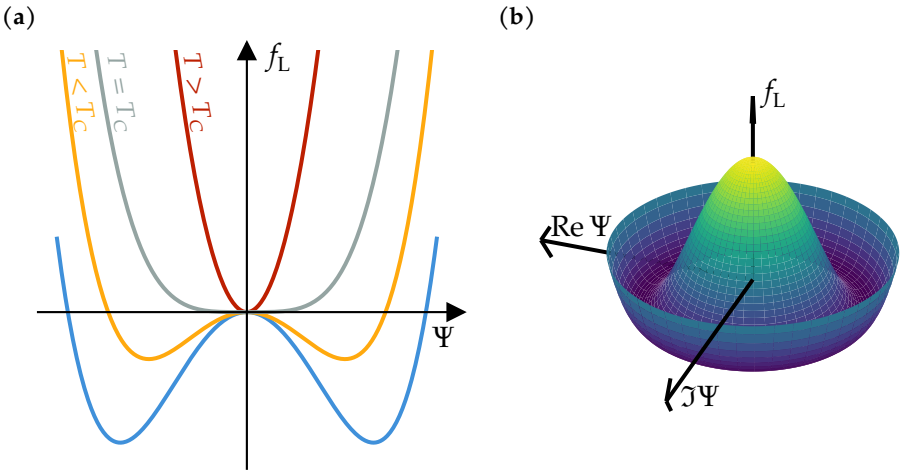

Figure 2.1 – Landau free energy and Mexican hat potential (**a**) Landau free energy f_L for a real-valued order parameter Ψ at different temperatures T. (**b**) Landau free energy for a complex order parameter Ψ.

The Landau free energy for a complex order parameter takes the form

$$f_L[\Psi] = r\Psi^*\Psi + \frac{u}{2}(\Psi^*\Psi)^2 = r|\Psi|^2 + \frac{u}{2}|\Psi|^4 \tag{2.10}$$

with again

$$r = a(T_C - T) \ . \tag{2.11}$$

Instead of the two minima, the free energy here has rotation symmetry, since it is independent of the phase of the order parameter:

$$f_L[\Psi] = f_L[e^{i\phi}\Psi] \ . \tag{2.12}$$

This results in the so called 'Mexican hat' potential shown in fig. 2.1b. In this potential, the phase of the order parameter can be rotated continuously, so that there is actually a continuum of symmetry-broken states.

In 1950, V. L. Ginzburg and L.D. Landau published their theory of superconductivity, based on Landaus theory of phase transitions [13]. Where Landau theory as described above has an uniform order parameter, Ginzburg-Landau theory accounts for it being spatially inhomogeneous, which in turn leads to the order parameter developing a fixed phase. As will be explained in this

section, this fixed phase is the underlying reason for the dissipationless flow in superfluid and superconductors.

The Ginzburg-Landau free energy for a complex order parameter is

$$f_{\mathrm{GL}}[\Psi, \Delta\Psi] = \frac{\hbar^2}{2m^*}|\Delta\Psi|^2 + r|\Psi|^2 + \frac{u}{2}|\Psi|^4 \,, \tag{2.13}$$

where the gradient term $\Delta\Psi$ is added in comparison to the Landau free energy. The prefactor $\frac{\hbar^2}{2m^*}$ is chosen to illustrate the interpretation of the Ginzburg-Landau free energy as the energy of a condensate of bosons, where the gradient term $|\Delta\Psi|^2$ is the kinetic energy.

The free energy in eq. (2.13) is sensitive to a twist of the phase of the order parameter. Writing $\Psi = |\Psi|e^{\mathrm{i}\phi}$, the gradient term reads

$$\Delta\Psi = (\Delta|\Psi| + \mathrm{i}\,\Delta\phi|\Psi|)e^{\mathrm{i}\phi} \,. \tag{2.14}$$

With that, eq. (2.13) becomes

$$f_{GL} = \frac{\hbar^2}{2m^*}|\Psi|^2(\Delta\phi)^2 + \left[\frac{\hbar^2}{2m^*}(\Delta|\Psi|)^2 + r|\Psi|^2 + \frac{u}{2}|\Psi|^4\right] . \tag{2.15}$$

Now the contributions of phase and amplitude variations are split up: the first term describes the energy cost of variations in the phase of the order parameter and the second term describes the energy cost of variations in the magnitude of the order parameter.

The dominating fluctuation is determined by the ratio of the factors $\frac{\hbar^2}{2m^*}$ and r, which has the dimension $(\mathrm{Length})^2$, from which one can define the correlation length

$$\xi = \sqrt{\frac{\hbar^2}{2m^*|r|}} = \xi_0\left(1 - \frac{T}{T_C}\right)^{-\frac{1}{2}} \tag{2.16}$$

with the zero temperature value defined as the coherence length $\xi_0 = \xi(T = 0) = \sqrt{\frac{\hbar^2}{2maT_C}}$. On length scales above ξ, the physics is entirely controlled by the phase degrees of freedom, i.e.:

$$f_{\mathrm{GL}} = \frac{\hbar^2}{2m^*}|\Psi|^2\,(\Delta\phi)^2 + \text{const.} \tag{2.17}$$

$$= \frac{\hbar^2}{4m^*}n_{\mathrm{S}}\,(\Delta\phi)^2 + \text{const.} \tag{2.18}$$

$$= D_{\mathrm{S}}\,(\Delta\phi)^2 + \text{const.} \tag{2.19}$$

where $\frac{n_S}{2} = |\Psi|^2$ is the density of single electrons which form the Cooper pairs, also called the superfluid or superconducting density. Equation (2.19) shows that twisting the phase of the condensate is associated with an energy cost. This energy cost is characterized by the superfluid phase stiffness D_S.

Assuming frozen amplitude fluctuations $\Delta|\Psi(\mathbf{r})| = 0$, the stationary point of eq. (2.15) is

$$|\Psi| = |\Psi_0|\sqrt{1 - \xi^2|\Delta\phi(\mathbf{r})|^2}\,. \tag{2.20}$$

This shows that the superconducting order gets suppressed and eventually destroyed by short-ranged (below ξ) phase fluctuations. By introducing a particular form of phase fluctuations $\phi = \mathbf{q}\cdot\mathbf{r}$ into a microscopic model, it is possible to probe this breakdown of superconductivity and thus gain insight into the nature of superconductivity, in particular this gives access to ξ. This method will be explained further in a later section.

The discussion so far is valid for neutral superfluids, but superconductors are charged superfluids, so they couple to electromagnetic fields. The Ginzburg-Landau free energy with minimal coupling to an electromagnetic field is

$$f_{\mathrm{GL}}[\Psi, \mathbf{A}] = \frac{\hbar^2}{2m^*}\left|\left(\Delta - \frac{\mathrm{i}e^*}{\hbar}\mathbf{A}\right)\Psi\right|^2 + r|\Psi|^2 + \frac{u}{2}|\Psi|^4 + \frac{B^2}{2\mu_0}\,. \tag{2.21}$$

with an additional term to include the electromagnetic energy of the magnetic field $\mathbf{B} = \nabla\times\mathbf{A}$. It describes two intertwined Ginzburg-Landau theories for Ψ and $\mathbf{A}$. This mean there are two length scales, the coherence length ξ governing amplitude fluctuations of Ψ and the London penetration depth λ_{L} which is associated with variations of the vector potential $\mathbf{A}$. This can be seen by considering a homogeneous condensate $\Psi = \sqrt{n_s/2}$, such that the free energy only depends on the vector potential as

$$f_{\mathrm{GL}}[\mathbf{A}] \sim \frac{e^2 n_s}{2m^*}A^2 + \frac{(\nabla\times\mathbf{A})^2}{2\mu_0} = \frac{1}{2\mu_0}\left(\frac{1}{\lambda_{\mathrm{L}}^2}A^2 + (\nabla\times\mathbf{A})^2\right) \tag{2.22}$$

with the London penetration depth

$$\lambda_L = \sqrt{\frac{m^*}{e^2 n_s \mu_0}} \tag{2.23}$$

as the prefactor of A^2, i.e. it is associated with the variations of $\mathbf{A}$. It is connected to the condensate stiffness as

$$\lambda_{\mathrm{L}} = \sqrt{\frac{m^*}{e^2 n_s \mu_0}} = \sqrt{\frac{\hbar^2}{4e^2\mu_0}\frac{4m^*}{\hbar^2 n_s}} = \sqrt{\frac{\hbar^2}{4e^2\mu_0}\frac{1}{D_s}}\,, \tag{2.24}$$

see eq. (2.19).

The current density can be calculated from the stationary point condition of the free energy w.r.t. the vector potential $\mathbf{A}$

$$\frac{\delta f_{\mathrm{GL}}}{\delta \mathbf{A}} = -\mathbf{j} + \frac{1}{\mu_0}\nabla \times \mathbf{B} \stackrel{!}{=} 0 \tag{2.25}$$

defining the supercurrent density

$$\mathbf{j} = -\mathrm{i}\frac{e\hbar}{m^*}\left(\Psi^* \Delta\Psi - \Psi \Delta\Psi^*\right) - \frac{4e^2}{m^*}|\Psi|^2\mathbf{A}\,. \tag{2.26}$$

Introducing the order parameter with a fixed phase $\Psi = |\Psi|e^{\mathrm{i}\phi}$ gives

$$\mathbf{j} = 2e|\Psi|^2\frac{\hbar}{m^*}\left(\nabla\phi - \frac{2\pi}{\Phi_0}\mathbf{A}\right) \tag{2.27}$$

with the magnetic flux quantum $\Phi_0 = \frac{\pi\hbar}{e}$. This shows that not only an applied field $\mathbf{A}$ can induce a supercurrent, but also the phase twist $\nabla\phi$ of the condensate ground state, which is the remarkable property of superconductors enabling the dissipationless current. Where a conventional current is achieved by excitations above the ground state, the superflow is achieved through deformation of the ground-state phase. The supercurrent can be gauge-transformed to

$$\mathbf{j} = -\frac{4e^2 n_S}{m^*}\mathbf{A} = \tilde{D}_S\mathbf{A} \tag{2.28}$$

which shows that the superfluid phase stiffness

$$D_{\mathrm{S}} = \frac{\hbar^2}{(2e)^2}\tilde{D}_S \tag{2.29}$$

also encodes the linear response of a system to a small applied vector field $\mathbf{A}$.

Calculating Superconducting Length Scales

As previously discussed in the context of eq. (2.20), analyzing the breakdown of the order parameter with phase fluctuations provides insight into the coherence length ξ_0 and the London penetration depth λ_L. A particular choice of phase fluctuations would be

$$\phi(\mathbf{r}) = \mathbf{q} \cdot \mathbf{r} \,, \tag{2.30}$$

which corresponds to Cooper pairs with a finite center-of-mass momentum $\mathbf{q}$. Although Cooper pairs typically do not carry such momentum in most materials, superconducting states with finite momentum can emerge under the influence of external fields or magnetism [14–16].

This approach for examining superconducting length scales that is also the was developed by Witt et al. [8]. The authors used the method to characterize superconductivity in alkali-doped fullerides, a material noted for its strong electronic correlations. They find that via multiorbital effects, a superconducting state characterized by a short coherence length yet robust stiffness, alongside a domeless increase in critical temperature with increasing pairing interaction This is in contrast to the usual BCS-BEC crossover phenomenology that can be seen in unconventional superconductors, where with increasing pairing interaction there is a maximum of the critical temperature. This shows that understanding superconducting length scales is particularly crucial in the characterization of new high T_C superconductors.

This section introduces the method within the framework of Ginzburg-Landau theory. The integration of this method into microscopic theories such as BCS theory and DMFT will be covered in the respective subsequent sections.

The phase fluctuation in eq. (2.30) corresponds to Fulde–Ferrell (FF) type pairing [17]

$$\Psi_\mathbf{q}(\mathbf{r}) = |\Psi_\mathbf{q}| e^{\mathrm{i}\mathbf{q}\mathbf{r}} \,. \tag{2.31}$$

With that, the free energy density eq. (2.13) is

$$f_{GL}[\Psi_\mathbf{q}] = r|\Psi_\mathbf{q}|^2 + \frac{u}{2}|\Psi_\mathbf{q}|^4 + \frac{\hbar^2 q^2}{2m^*}|\Psi_\mathbf{q}|^2 \,. \tag{2.32}$$

The stationary point of the system can again be found via the condition

$$\frac{\delta f_{GL}}{\delta \Psi_\mathbf{q}^*} = 2\Psi_\mathbf{q}\left[r(1-\xi^2 q^2) + u|\Psi_\mathbf{q}|^2\right] = 0 \,, \tag{2.33}$$

which results in the **q**-dependence of the order parameter

$$|\Psi_{\mathbf{q}}|^2 = |\Psi_0|^2 \left(1 - \xi(T)^2 q^2\right) . \tag{2.34}$$

This can be seen in fig. 2.2a. So for some value $\mathbf{q}_c$, the kinetic energy from phase modulations exceeds the gain in energy from pairing and superconducting order breaks down

$$\psi_{\mathbf{q}_c} = 0 . \tag{2.35}$$

So in Ginzburg-Landau theory the correlation length can be calculated via

$$q_c = \xi(T)^{-1} . \tag{2.36}$$

The temperature dependence of the $\xi(T)$ then gives access to the coherence length via eq. (2.16)

$$\xi(T) = \xi_0 \left(1 - \frac{T}{T_C}\right)^{-\frac{1}{2}} \tag{2.37}$$

Equation (2.26) shows that the momentum of the Cooper pairs entails a supercurrent $\mathbf{j}_{\mathbf{q}}$. With $\phi(\mathbf{r}) = \mathbf{q} \cdot \mathbf{r}$ and $\mathbf{A} = 0$, the current is

$$\mathbf{j}_{\mathbf{q}} = \frac{2\hbar e}{m^*} |\Psi_{\mathbf{q}}|^2 \mathbf{q} . \tag{2.38}$$

The current $\mathbf{j}_{\mathbf{q}}$ is a non-monotonous function of **q** with a maximum called the depairing current j_{dp} as can be seen in fig. 2.2b. The depairing current is an upper boundary for the maximal current that can flow through a material, also called the critical current j_c. The value of j_c is strongly dependent on the geometry of the sample [18, 19], so j_{dp} is not necessarily experimentally available, but it can be used to calculate the London penetration depth [4]

$$\lambda_{\mathrm{L}}(T) = \sqrt{\frac{\Phi_0}{3\sqrt{3}\pi\mu_0 \xi(T) j_{\mathrm{dp}}(T)}} = \lambda_{L,0} \left(1 - \left(\frac{T}{T_{\mathrm{C}}}\right)\right)^{-\frac{1}{2}} . \tag{2.39}$$

The superfluid phase stiffness can then be calculated via eq. (2.24)

$$D_S \propto \lambda_{\mathrm{L}}^{-2} . \tag{2.40}$$

The finite-momentum method in the limit of $\mathbf{q} \to 0$ is related to linear response techniques to calculate the superfluid weight [9, 20].

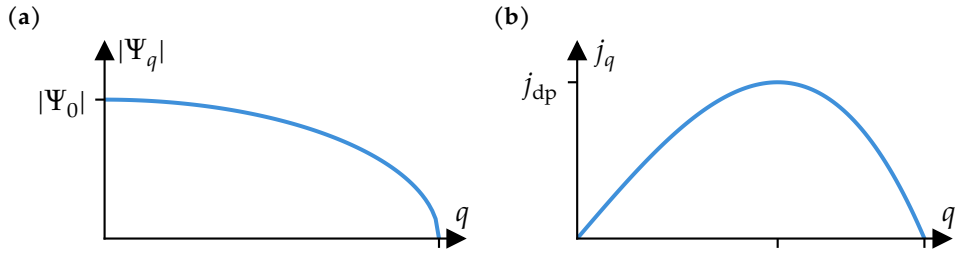

Figure 2.2 – Ginzburg-Landau solutions for a finite momentum q. **(a)** Breakdown of the order parameter with q, the critical q_c is the point at which the order parameter is 0. **(b)** Superconducting current coming from the finite momentum of the Cooper pairs. The maximum of the current with q is called the depairing current j_{dp}.

2.2 Bardeen-Coooper-Schrieffer Theory

The BCS (Bardeen-Cooper-Schrieffer) description of superconductivity was the first microscopic theory, identifying condensation of electrons into pairs forming a macroscopic quantum state as the underlying mechanism [21]. The BCS-Hamiltonian is

$$H_{\mathrm{BCS}} = \sum_{\mathbf{k}\sigma} \epsilon_{\mathbf{k}\sigma} c^\dagger_{\mathbf{k}\sigma} c_{\mathbf{k}\sigma} + \sum_{\mathbf{k},\mathbf{k}'} V_{\mathbf{k},\mathbf{k}'} c^\dagger_{\mathbf{k}\uparrow} c^\dagger_{-\mathbf{k}\downarrow} c_{-\mathbf{k}'\downarrow} c_{\mathbf{k}'\uparrow} \,, \tag{2.41}$$

where $V_{\mathbf{k},\mathbf{k}'}$ is a model interaction. It describes a phonon-mediated attractive interaction for energies lower than the Debye frequency ω_{D}:

$$V_{\mathbf{k},\mathbf{k}'} = \begin{cases} -V_0 & (\epsilon_{\mathbf{k}}, \epsilon_{\mathbf{k}'} < \omega_{\mathrm{D}}) \\ 0 & (\text{otherwise}) \end{cases} . \tag{2.42}$$

The BCS Hamiltonian can be treated in a mean-field approach, writing

$$\begin{aligned} \sum_{\mathbf{k},\mathbf{k}'} V_{\mathbf{k},\mathbf{k}'} c^\dagger_{\mathbf{k}\uparrow} c^\dagger_{-\mathbf{k}\downarrow} c_{-\mathbf{k}'\downarrow} c_{\mathbf{k}'\uparrow} &\approx \sum_{\mathbf{k},\mathbf{k}'} V_{\mathbf{k},\mathbf{k}'} \langle c^\dagger_{\mathbf{k}\uparrow} c^\dagger_{-\mathbf{k}\downarrow} \rangle c_{-\mathbf{k}'\downarrow} c_{\mathbf{k}'\uparrow} + V_{\mathbf{k},\mathbf{k}'} c^\dagger_{\mathbf{k}\uparrow} c^\dagger_{-\mathbf{k}\downarrow} \langle c_{-\mathbf{k}'\downarrow} c_{\mathbf{k}'\uparrow} \rangle \\ &= \sum_{\mathbf{k}} \Delta^*_{\mathbf{k}} c_{-\mathbf{k}\downarrow} c_{\mathbf{k}\uparrow} + \Delta_{\mathbf{k}} c^\dagger_{\mathbf{k}\uparrow} c^\dagger_{-\mathbf{k}\downarrow} \end{aligned} \tag{2.43}$$

with the pairing amplitude

$$\Delta_{\mathbf{k}} = -\sum_{\mathbf{k}'} V_{\mathbf{k},\mathbf{k}'} \langle c_{-\mathbf{k}'\downarrow} c_{\mathbf{k}'\uparrow} \rangle \,, \tag{2.44}$$

which is also the order parameter in BCS theory. A finite Δ corresponds to the pairing introduced above: it means there is a finite expectation value for a coherent creation/annihilation of electron pairs with opposite momentum and spin.

BCS theory was very successful in two ways: on the one hand it could quantitatively explain effects in the superconductors known at the time, for example the Hebel-Slichter peak that was measured in 1957 [22, 23] and the band gap measured by Giaever in 1960 [24]. On the other hand it gave a microscopic explanation for the phenomenological theories of superconductivity based on F. Londons 1937 description of a quantum-mechanical wave function with a defined phase [25]. This picture of electron pairing still holds today even for superconductors that cannot be described by BCS theory [26].

There exist many textbooks tackling BCS theory from different angles, such as refs. [3, 4]. This section will use the ideas from BCS theory to treat superconductivity in the attractive Hubbard model on a mean-field level.

Multiband BCS Theory

The Hubbard model is regarded as the simplest model for interacting electron systems. It goes back to works by Hubbard [27], Kanamori [28] and Gutzweiler [29] in the 1960s. The Hamiltonian of the single-band Hubbard model is

$$H = H_0 + H_{\text{int}} = \sum_{\langle ij\rangle\sigma} \left(-t_{ij} - \mu_\sigma \delta_{ij}\right) c^\dagger_{i\sigma} c_{j\sigma} + \text{h.c.} + U \sum_i c^\dagger_{i\uparrow} c^\dagger_{i\downarrow} c_{i\downarrow} c_{i\uparrow} \qquad (2.45)$$

where $U > 0$. The interaction describes a repulsive interaction between electrons of different spin at the same lattice site.

The Hubbard interaction is localized to one lattice site, so the Hubbard model emphasizes the electronic correlations due to local interactions. With the discovery of high T_C superconductors in the Cuprates, it was quickly realized that the 2D Hubbard model in the intermediate to strong-coupling regime could describe the CuO_2 layers [30] well. Just as Cuprate materials, the Hubbard model has parameter regimes with $d_{x^2-y^2}$ superconductivity, strong antiferromagnetic correlations, stripe order, pseudogaps, Fermi liquid and bad metallic behavior, with the phase diagram lines and observables being similar as a function of doping and temperature. Besides the relevancy for the Cuprates, having few parameters and simultaneously a very rich phase diagram with a variety of many-body effects also made the Hubbard model a perfect playground for new

numerical tools, among them diagonalization, diagrammatics, tensor network, Quantum Monte Carlo (QMC) methods and DMFT (see section 2.3) [31].

The Hubbard model in the form of eq. (2.45) can be extended in a multitude of ways to model a variety of physical system, in this thesis to multiple orbitals (i.e. atoms in the unit cell for lattice systems) and an attractive interaction. The local attractive interaction in this extended Hubbard model is useful as a model with a simple set of parameters to study superconductivity in systems where electrons experience a strong local attractive interaction mediated through phonon degrees of freedom or with electronic excitations [32]. The form of the Hubbard Hamiltonian is then

$$H = \sum_{\langle i\alpha j\beta\rangle\sigma} \left(-t_{i\alpha,j\beta} - \mu_\sigma \delta_{i\alpha,j\beta}\right) c^\dagger_{i\alpha\sigma} c_{j\beta\sigma} + \text{h.c.} - \sum_{i,\alpha} U_\alpha c^\dagger_{i\alpha\uparrow} c^\dagger_{i\alpha\downarrow} c_{i\alpha\downarrow} c_{i\alpha\uparrow} \,, \quad (2.46)$$

where α counts orbitals and the minus sign in front of the interaction term is taken as a convention so that $U > 0$ now corresponds to an attractive interaction.

The idea of the mean-field approximation relies on the assumption that operators A do not deviate much from their average value $\langle A\rangle$, meaning the deviation $\delta A = A - \langle A\rangle$ are small. Looking at the interaction term eq. (2.46) and taking the idea of pairing from the BCS Hamiltonian, the deviation operators for pair creation/annihilation operators are

$$\begin{aligned} d_{i\alpha} &= c^\dagger_{i\alpha\uparrow} c^\dagger_{i\alpha\downarrow} - \langle c^\dagger_{i\alpha\uparrow} c^\dagger_{i\alpha,\downarrow}\rangle \\ e_{i\alpha} &= c_{i\alpha\downarrow} c_{i\alpha\uparrow} - \langle c_{i\alpha\downarrow} c_{i\alpha\uparrow}\rangle \,. \end{aligned} \quad (2.47)$$

Using these, the interaction part of the Hamiltonian becomes

$$H_{\text{int}} = -\sum_{i,\alpha} U_\alpha c^\dagger_{i\alpha\uparrow} c^\dagger_{i\alpha\downarrow} c_{i\alpha\downarrow} c_{i\alpha\uparrow} \quad (2.48)$$

$$= -\sum_{i,\alpha} U_\alpha \left(d^\dagger_{i\alpha} + \langle c^\dagger_{i\alpha\uparrow} c^\dagger_{i\alpha\downarrow}\rangle\right)\left(e_{i\alpha} + \langle c_{i\alpha\downarrow} c_{i\alpha\uparrow}\rangle\right) \quad (2.49)$$

$$\begin{aligned} = -\sum_{i,\alpha} U_\alpha (& d_{i\alpha} e_{i\alpha} + d_{i,\alpha} \langle c_{i\alpha,\downarrow} c_{i\alpha\uparrow}\rangle \\ &+ e_{i\alpha} \langle c^\dagger_{i\alpha,\uparrow} c^\dagger_{i\alpha\downarrow}\rangle + \langle c^\dagger_{i\alpha\uparrow} c^\dagger_{i\alpha\downarrow}\rangle \langle c_{i\alpha\downarrow} c_{i\alpha\uparrow}\rangle) \,, \end{aligned} \quad (2.50)$$

where the first term is quadratic in the deviations and can be neglected. Thus one arrives at the approximation

$$\begin{aligned} H_{\text{int}} \approx & -\sum_{i,\alpha} U_\alpha \left(d_{i\alpha} \langle c_{i\alpha,\downarrow} c_{i\alpha\uparrow} \rangle + e_{i\alpha} \langle c^\dagger_{i\alpha\uparrow} c^\dagger_{i\alpha\downarrow} \rangle \right. \\ & \left. + \langle c^\dagger_{i\alpha\uparrow} c^\dagger_{i\alpha\downarrow} \rangle \langle c_{i\alpha\downarrow} c_{i\alpha\uparrow} \rangle \right) \qquad (2.51) \\ = & -\sum_{i,\alpha} U_\alpha \left(c^\dagger_{i\alpha\uparrow} c^\dagger_{i\alpha\downarrow} \langle c_{i\alpha\downarrow} c_{i\alpha\uparrow} \rangle + c_{i\alpha\downarrow} c_{i\alpha\uparrow} \langle c^\dagger_{i\alpha\uparrow} c^\dagger_{i\alpha\downarrow} \rangle \right. \\ & \left. - \langle c^\dagger_{i\alpha\uparrow} c^\dagger_{i\alpha\downarrow} \rangle \langle c_{i\alpha\downarrow} c_{i\alpha\uparrow} \rangle \right) \qquad (2.52) \\ = & \sum_{i,\alpha} \left(\Delta_{i\alpha} c^\dagger_{i\alpha\uparrow} c^\dagger_{i\alpha\downarrow} + \Delta^*_{i\alpha} c_{i\alpha\downarrow} c_{i\alpha\uparrow} - \frac{|\Delta_{i\alpha}|^2}{U_\alpha} \right) \qquad (2.53) \end{aligned}$$

with the local superconducting order parameter

$$\Delta_{i,\alpha} = -U_\alpha \langle c_{i\alpha\downarrow} c_{i\alpha\uparrow} \rangle \ . \qquad (2.54)$$

This results in the mean-field Hamiltonian

$$\begin{aligned} H_{\text{MF}} = & \sum_{\langle i\alpha j\beta \rangle \sigma} \left(-t_{i\alpha,j\beta} - \mu_\sigma \delta_{i\alpha,j\beta} \right) c^\dagger_{i\alpha,\sigma} c_{j\beta,\sigma} + \text{h.c.} \\ & + \sum_{i,\alpha} \left(\Delta_{i\alpha} c^\dagger_{i\alpha\uparrow} c^\dagger_{i\alpha\downarrow} + \Delta^*_{i\alpha} c_{i\alpha\downarrow} c_{i\alpha\uparrow} - \frac{|\Delta_{i\alpha}|^2}{U_\alpha} \right) \qquad (2.55) \end{aligned}$$

To include finite momentum in BCS theory, take the ansatz of a Fulde-Ferrel (FF) type pairing [17]:

$$\Delta_{i,\alpha} = \Delta_\alpha e^{\mathrm{i}\mathbf{q}\mathbf{r}_{i\alpha}} \qquad (2.56)$$

The mean-field Hamiltonian can be written in momentum space using the Fourier transform

$$c_{i\alpha\sigma} = \frac{1}{\sqrt{N}} \sum_{\mathbf{k}} e^{\mathrm{i}\mathbf{k}\mathbf{r}_{i\alpha}} c_{\mathbf{k}\alpha\sigma} \ , \qquad (2.57)$$

with position vectors $\mathbf{r}_{i\alpha} = \mathbf{R}_i + \delta_\alpha$, written using the position of the unit cell $\mathbf{R}_i$ and the orbital position inside the unit cell δ_α. Using this, the mean-field Hamiltonian is

$$H_{\text{MF}}(\mathbf{q}) = \sum_{\mathbf{k}} \Psi^\dagger_{\mathbf{q},\mathbf{k}} H_{\text{BdG}}(\mathbf{q},\mathbf{k}) \Psi_{\mathbf{q},\mathbf{k}} + K_{\mathbf{q}} \qquad (2.58)$$

with the Nambu spinors

$$\Psi_{\mathbf{q},\mathbf{k}} = \begin{pmatrix} c_{\mathbf{k}1\uparrow} & c_{\mathbf{k}2\uparrow} & \dots & c_{\mathbf{k}n_{\mathrm{orb}}\uparrow} & c^{\dagger}_{\mathbf{q}-\mathbf{k}1\downarrow} & c^{\dagger}_{\mathbf{q}-\mathbf{k}2\downarrow} & \dots & c^{\dagger}_{\mathbf{q}-\mathbf{k}n_{\mathrm{orb}}\downarrow} \end{pmatrix}^{T} \tag{2.59}$$

and

$$K_{\mathbf{q}} = \sum_{\mathbf{k}} \mathrm{Tr}[H^{\downarrow}_{\mathbf{k}}] - n_{\mathrm{orb}} N\mu - N \sum_{\alpha} \frac{|\Delta_{\alpha}(\mathbf{q})|^2}{U} \,. \tag{2.60}$$

The matrix between the spinors is the so-called Bogoliubov-de Gennes (BdG) matrix

$$H_{\mathrm{BdG}}(\mathbf{q},\mathbf{k}) = \begin{pmatrix} H^{\uparrow}_{\mathbf{k}} - \mu & \Delta(\mathbf{q}) \\ \Delta^{\dagger}(\mathbf{q}) & -\left(H^{\downarrow}_{\mathbf{q}-\mathbf{k}}\right)^{*} + \mu \end{pmatrix} \tag{2.61}$$

with $H_{0,\sigma}$ being the F.T. of the kinetic term

$$[H^{\sigma}_{\mathbf{k}}] = \sum_{i} t^{\sigma}_{i\alpha,0\beta} e^{-\mathbf{i}\mathbf{k}\cdot(\mathbf{R}_i + \delta_{\alpha} - \delta_{\beta})} \tag{2.62}$$

and the matrix of order parameters, with the $\mathbf{q}$-dependence made explicit:

$$\Delta = \mathrm{diag}(\Delta_1(\mathbf{q}), \Delta_2(\mathbf{q}), \dots, \Delta_{n_{\mathrm{orb}}}(\mathbf{q})) \,. \tag{2.63}$$

For time-reversal symmetric systems, there exists a solution such that all Δ_{α} are real [9] but the introduction of a finite $\mathbf{q}$ breaks time-reversal symmetry. This means that in a multiband system, the order parameters in the orbital can develop different phases.

In the BdG formulation, the problem is now reduced to diagonalization of the matrix in eq. (2.61), so one can write

$$H_{\mathrm{BdG}} = U_{\mathbf{q},\mathbf{k}} \epsilon_{\mathbf{q},\mathbf{k}} U^{\dagger}_{\mathbf{q},\mathbf{k}} \tag{2.64}$$

with the diagonal matrix $\epsilon_{\mathbf{q},\mathbf{k}} = \mathrm{diag}(\epsilon_1(\mathbf{q},\mathbf{k}), \epsilon_2(\mathbf{q},\mathbf{k}), \dots, \epsilon_{2\cdot n_{\mathrm{orb}}}(\mathbf{q},\mathbf{k}))$.

The BdG formulation defines a linear transformation from the creation and annihilation to a new set of operators

$$\gamma_{\mathbf{q},\mathbf{k}} = \begin{pmatrix} \gamma_{\mathbf{q},\mathbf{k},1} & \gamma_{\mathbf{q},\mathbf{k},2} & \cdots & \gamma_{\mathbf{q},\mathbf{k},2\cdot n_{\mathrm{orb}}} \end{pmatrix}^{T} \tag{2.65}$$

via

$$\gamma_{\mathbf{q},\mathbf{k}} = U^{\dagger}_{\mathbf{q},\mathbf{k}} \Psi_{\mathbf{q},\mathbf{k}} \tag{2.66}$$

which define non-interacting quasi-particles. Using these operators, the mean-field Hamiltonian becomes

$$H_{\mathrm{MF}}(\mathbf{q}) = \sum_{\mathbf{k}} \gamma_{\mathbf{q},\mathbf{k}} \epsilon_{\mathbf{q},\mathbf{k}} \gamma^{\dagger}_{\mathbf{q},\mathbf{k}} \tag{2.67}$$

Mean-field theory does not give a value for the order parameter a priori, it needs to be calculated self-consistently using the gap equation

$$\begin{aligned} \Delta_\alpha &= -U_\alpha \langle c_{i\alpha\downarrow} c_{i\alpha\uparrow} \rangle = -\frac{U}{N} \sum_{\mathbf{k}} \langle c_{\mathbf{k}\alpha\downarrow} c_{-\mathbf{k}\alpha\uparrow} \rangle \\ &= -\frac{U}{N} \sum_{\mathbf{k}} \sum_{ij} [U^{\dagger}_{\mathbf{q},\mathbf{k}}]_{i,\alpha+n_{\mathrm{orb}}} [U_{\mathbf{q},\mathbf{k}}]_{\alpha,j} \langle \gamma^{\dagger}_i \gamma_i \rangle \\ &= -\frac{U}{N} \sum_{\mathbf{k}} [U_{\mathbf{q},\mathbf{k}} n_{\mathrm{F}}(\epsilon_{\mathbf{q},\mathbf{k}}) U^{\dagger}_{\mathbf{q},\mathbf{k}}]_{\alpha,\alpha+n_{\mathrm{orb}}} . \end{aligned} \tag{2.68}$$

This means starting from an initial value, the BdG matrix needs to be set up, diagonalized and then used to determine Δ_α again, until a converged value is found.

To implement the finite $\mathbf{q}$ method to calculate the superconducting length scales, one also needs access to the supercurrent in BCS theory. In general, a current $\mathbf{j}$ is induced by change of the local polarization $\mathbf{P}$. The polarization operator given by

$$\hat{\mathbf{P}} = e \sum_{i\alpha} \mathbf{R}_{i\alpha} c^{\dagger}_{i\alpha} c_{i\alpha} = e \sum_{i\alpha} \mathbf{R}_{i\alpha} n_{i\alpha} , \tag{2.69}$$

so that the current given by the time derivative of the polarization operator is

$$\hat{\mathbf{j}} = \dot{\hat{\mathbf{P}}} = \frac{\mathrm{i}}{\hbar} [\hat{\mathbf{P}}, H] . \tag{2.70}$$

Taking a Hamiltonian with pairing $\Delta_{i\alpha}$

$$H = \sum_{\langle i\alpha j\beta \rangle \sigma} -t_{i\alpha,j\beta} c^{\dagger}_{i\alpha\sigma} c_{j\beta\sigma} + \sum_{i,\alpha} \left(\Delta_{i\alpha} c^{\dagger}_{i\alpha\uparrow} c^{\dagger}_{i\alpha\downarrow} + \Delta^{*}_{i\alpha} c_{i\alpha\downarrow} c_{i\alpha\uparrow} \right) =: H_{\mathrm{N}} + H_{\mathrm{AN}} \tag{2.71}$$

one needs to calculate three kinds of commutators for eq. (2.70):

$$[n_{m\gamma}, c^{\dagger}_{i\alpha} c_{j\beta}] = c^{\dagger}_{i\alpha} [n_{m\gamma}, c_{j\beta}] + [n_{m\gamma}, c^{\dagger}_{i\alpha}] c_{j\beta} = (\delta_{m\gamma,i\alpha} - \delta_{m\gamma,j\beta}) c^{\dagger}_{i\alpha} c_{j\beta} \tag{2.72}$$

$$[n_{m\gamma}, c_{i\alpha} c_{i\alpha}] = c_{i\alpha} [n_{m\gamma}, c_{i\alpha}] + [n_{m\gamma}, c_{i\alpha}] c_{i\alpha} = -2\delta_{m\gamma,i\alpha} c_{i\alpha} c_{i\alpha} \tag{2.73}$$

$$[n_{m\gamma}, c^{\dagger}_{i\alpha} c^{\dagger}_{i\alpha}] = c^{\dagger}_{i\alpha} [n_{m\gamma}, c^{\dagger}_{i\alpha}] + [n_{m\gamma}, c^{\dagger}_{i\alpha}] c^{\dagger}_{i\alpha} = 2\delta_{m\gamma,i\alpha} c^{\dagger}_{i\alpha} c^{\dagger}_{i\alpha} . \tag{2.74}$$

Using these, the normal and anomalous component of the current can be calculated:

$$\begin{aligned}
\hat{\mathbf{j}}_{\mathrm{N}} &= \frac{i}{\hbar}[\hat{\mathbf{P}}, H_{\mathrm{N}}] = -\mathrm{i}\frac{e}{\hbar}\sum_{i\alpha,j\beta,m\gamma}\mathbf{R}_{m\gamma}t_{i\alpha,j\beta}[n_{m\gamma}, c^{\dagger}_{i\alpha}c_{j\beta}] \\
&= -\mathrm{i}\frac{e}{\hbar}\sum_{i\alpha,j\beta,m\gamma}\mathbf{R}_{m\gamma}t_{i\alpha,j\beta}(\delta_{m\gamma,i\alpha}-\delta_{m\gamma,j\beta})c^{\dagger}_{i\alpha}c_{j\beta} \\
&= -\mathrm{i}\frac{e}{\hbar}\sum_{i\alpha,j\beta}(\mathbf{R}_{i\alpha}-\mathbf{R}_{j\beta})t_{i\alpha,j\beta}c^{\dagger}_{i\alpha}c_{j\beta} \qquad (2.75) \\
\hat{\mathbf{j}}_{\mathrm{AN}} &= \frac{i}{\hbar}[\hat{\mathbf{P}}, H_{\mathrm{AN}}] = -\mathrm{i}\frac{e}{\hbar}\sum_{i\alpha,m\gamma}\mathbf{R}_{m\gamma}(\Delta_{i\alpha}[n_{m\gamma}, c_{i\alpha}c_{i\alpha}] + \Delta^{*}_{i\alpha}[n_{m\gamma}, c^{\dagger}_{i\alpha}c^{\dagger}_{i\alpha}] \\
&= -\mathrm{i}\frac{2e}{\hbar}\sum_{i\alpha,m\gamma}\mathbf{R}_{m\gamma}(-\delta_{m\gamma,i\alpha}\Delta_{i\alpha}c_{i\alpha}c_{i\alpha} + \delta_{m\gamma,i\alpha}\Delta^{*}_{i\alpha}c^{\dagger}_{i\alpha}c^{\dagger}_{i\alpha}) \\
&= \mathrm{i}\frac{2e}{\hbar}\sum_{i\alpha}\mathbf{R}_{i\alpha}(-\Delta_{i\alpha}c_{i\alpha}c_{i\alpha} + \Delta^{*}_{i\alpha}c^{\dagger}_{i\alpha}c^{\dagger}_{i\alpha})\,. \qquad (2.76)
\end{aligned}$$

The expectation value of the anomalous part vanishes

$$\begin{aligned}
\langle\hat{\mathbf{j}}_{\mathrm{AN}}\rangle &= \mathrm{i}\frac{2e}{\hbar}\sum_{i\alpha}\mathbf{R}_{i\alpha}(-\Delta_{i\alpha}\langle c_{i\alpha}c_{i\alpha}\rangle + \Delta^{*}_{i\alpha}\langle c^{\dagger}_{i\alpha}c^{\dagger}_{i\alpha}\rangle) \qquad (2.77) \\
&= \mathrm{i}\frac{2e}{\hbar}\sum_{i\alpha}\mathbf{R}_{i\alpha}(-\Delta_{i\alpha}\Delta^{*}_{i\alpha} + \Delta^{*}_{i\alpha}\Delta_{i\alpha}) = 0\,, \qquad (2.78)
\end{aligned}$$

so that the current density is given by the normal component.

Using the Fourier transform

$$c_{i\alpha\sigma} = \frac{1}{\sqrt{N}}\sum_{\mathbf{k}}e^{\mathrm{i}\mathbf{k}\mathbf{r}_{i\alpha}}c_{\mathbf{k}\alpha\sigma}\,, \qquad (2.79)$$

the current can be written as

$$\hat{\mathbf{j}} = \hat{\mathbf{j}}_{\mathrm{N}} = \mathrm{i}\frac{e}{\hbar}\frac{1}{N_k}\sum_{i\alpha,j\beta,vbk\mathbf{k}'}(\mathbf{R}_{i\alpha}-\mathbf{R}_{j\beta})t_{i\alpha,j\beta}e^{\mathrm{i}(\mathbf{k}\mathbf{r}_{i\alpha}-\mathbf{k}'\mathbf{r}_{j\alpha})}c^{\dagger}_{\mathbf{k}\alpha}c_{\mathbf{k}'\beta} \tag{2.80}$$

$$= \mathrm{i}\frac{e}{\hbar}\frac{1}{N_k}\sum_{i\alpha,j\beta,\mathbf{k}\mathbf{k}'}(\mathbf{R}_{i\alpha}-\mathbf{R}_{j\beta})t_{i\alpha,j\beta}e^{\mathrm{i}(\mathbf{k}\mathbf{r}_{i\alpha}-\mathbf{k}'\mathbf{r}_{j\alpha})}c^{\dagger}_{\mathbf{k}\alpha}c_{\mathbf{k}'\beta} \tag{2.81}$$

$$\overset{\mathbf{r}_{i\alpha}\mapsto\mathbf{r}_{i\alpha}+\mathbf{r}_{j\beta}}{=} \mathrm{i}\frac{e}{\hbar}\frac{1}{N_k}\sum_{\mathbf{r}_{i\alpha}\mathbf{k}\mathbf{k}'\alpha\beta\sigma}\mathbf{R}_{i\alpha}t_{i\alpha,j\beta}\sum_{\mathbf{r}_{j\beta}}e^{\mathrm{i}(\mathbf{k}-\mathbf{k}'\mathbf{r}_{j\beta}}c^{\dagger}_{\mathbf{k}\alpha}c_{\mathbf{k}'\beta} \tag{2.82}$$

$$= \frac{e}{\hbar N_k}\sum_{\mathbf{k}\alpha\beta\sigma}\mathrm{i}\sum_{\mathbf{r}_{i\alpha}}\mathbf{r}_{i\alpha}t_{\alpha\beta}e^{\mathrm{i}\mathbf{k}\mathbf{r}_{i\alpha}}c^{\dagger}_{\mathbf{k}\alpha}c_{\mathbf{k}\beta} = \frac{e}{\hbar N_k}\sum_{\mathbf{k}\alpha\beta\sigma}\nabla_{\mathbf{k}}h(\mathbf{k})_{\alpha\beta}c^{\dagger}_{\mathbf{k}\alpha}c_{\mathbf{k}\beta} \tag{2.83}$$

$$:= \frac{e}{N_k}\sum_{\mathbf{k}\alpha\beta\sigma}\mathbf{v}_{\alpha\beta}c^{\dagger}_{\mathbf{k}\alpha}c_{\mathbf{k}\beta} \tag{2.84}$$

This means current density is

$$\mathbf{j}_{\mathbf{q}} = \langle\hat{\mathbf{j}}\rangle_{\mathbf{q}} = \frac{e}{N_{\mathbf{k}}}\sum_{\mathbf{k}\alpha\beta\sigma}\mathbf{v}_{\alpha\beta}(\mathbf{k})\left\langle c^{\dagger}_{\mathbf{k}\alpha\sigma}c_{\mathbf{k}\beta\sigma}\right\rangle_{\mathbf{q}} = \frac{2e}{N_{\mathbf{k}}}\sum_{\mathbf{k}\alpha\beta}\mathbf{v}_{\alpha\beta}(\mathbf{k})\left\langle c^{\dagger}_{\mathbf{k}\alpha\uparrow}c_{\mathbf{k}\beta\uparrow}\right\rangle_{\mathbf{q}}\ , \tag{2.85}$$

which can be expressed using the BdG energies

$$\mathbf{j}_{\mathbf{q}} = \frac{2e}{N_{\mathbf{k}}}\sum_{\mathbf{k}\alpha\beta n}\mathbf{v}_{\alpha\beta}(\mathbf{k})[U_{\mathbf{q}\mathbf{k}}]_{\alpha n}[U^{*}_{\mathbf{q}\mathbf{k}}]_{\beta n}n_F(E_n)\ , \tag{2.86}$$

where $n \in \{1,\dots,2N_{\mathrm{orb}}\}$.

2.3 Dynamical Mean-Field Theory

The foundational idea of Dynamical Mean Field Theory (DMFT) is to map the full interacting problem to the problem of a single lattice site (or a small cluster of lattice sites) embedded in a mean field encompassing all non-local correlation effects. This mapping can be seen in fig. 2.3. In contrast to static mean-field theories such as BCS theory, DMFT treats all local correlations. When the interaction strength becomes comparable to the kinetic energy of the electrons, the electrons are becoming increasingly localized and the band structure picture is not applicable anymore. One hallmark effect in this strongly-correlated regime is the interaction driven metal-insulator (Mott) transition. Using DMFT,

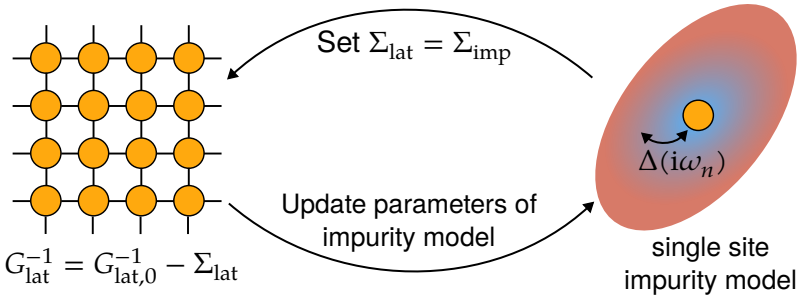

Figure 2.3 – Mapping of the full lattice problem onto a single-site impurity model. This also visualizes the DMFT self-consistency loop: Coming from the full lattice problem, an impurity model is set up, which is then solved to get the self-energy Σ_{imp}, which encompasses all interaction effects. The loop is converged when $\Sigma_{\text{lat}} = \Sigma_{\text{imp}}$, otherwise the impurity self-energy is a new guess for the self-energy of the lattice problem.

the Mott transition seen in materials like V_2O_3 [33] can be explained in the Hubbard model [34].

In this section I will describe the Green's function formalism, the mapping of the lattice problem onto the impurity problem and the resulting self-consistency loop of DMFT. Additionally, I will also describe how to treat the superconducting state in terms of Green's function and the consequences for the DMFT self-consistency condition. I will not fully derive the equations of DMFT here, for a more expansive introduction see refs. [3, 5, 35, 36].

Green's Function Formalism

Green's functions are a method to encode influence of many-body effects on propagation of particles in a system. Depending on the context different kinds of Green's functions are employed. Matsubara Green's functions naturally includes finite temperatures, which is done via a Wick rotation of the time variable t into imaginary time

$$t \to -i\tau \tag{2.87}$$

where τ is real and has the dimension time. This enables the simultaneous expansion of exponential $e^{-\beta H}$ coming from the thermodynamic average and e^{-iHt} coming from the time evolution of operators. Matsubara Greens function

are defined as

$$G_{\alpha_1\alpha_2}(\tau_1,\tau_2) = -\left\langle T_\tau(c_{\alpha_1}(\tau_1)c^\dagger_{\alpha_2}(\tau_2))\right\rangle \tag{2.88}$$

with:

- $c_\alpha, c^\dagger_\alpha$ fermionic creation/annihilation operators of quantum states α in the Heisenberg time-evolution picture $\hat{A}(\tau) = e^{\tau H}\hat{A}e^{-\tau H}$
- $\langle\cdot\rangle = \mathrm{Tr}(\hat{\rho}\,\cdot)$ the thermal expectation value with statistical operator $\hat{\rho} = {}^{e^{-\beta H}}/_{Z}$ with partition function Z and Hamiltonian H
- Time-ordering operator

$$\begin{aligned} T_\tau(A(\tau)B(\tau')) &= \Theta(\tau-\tau')A(\tau)B(\tau') \pm \Theta(\tau'-\tau)B(\tau')A(\tau) \\ &= \begin{cases} A(\tau)B(\tau') & \text{if } \tau > \tau' \\ B(\tau')A(\tau) & \text{if } \tau' > \tau \end{cases} \end{aligned} \tag{2.89}$$

In thermal equilibrium, the Green's function only depends on time differences $\tau_1 - \tau_2$, so by defining $\tau = \tau_1 - \tau_2$, one can work with a single time.

Fermionic Matsubara Green's functions are antiperiodic in time with periodicity β. For $-\beta < 0 < 0$, the cyclic properties of the trace means that

$$G(\tau) = -G(\tau+\beta)\ . \tag{2.90}$$

This means that the Green's functions can be restricted to the interval $0 < \tau < \beta$ and in turn, there is a Fourier expansion with discrete frequencies $\omega_n = {}^{(2n+1)\pi}/_{\beta}$:

$$G(\mathrm{i}\omega_n) = \int_0^\beta \mathrm{d}\tau G(\tau)e^{\mathrm{i}\omega_n\tau} \tag{2.91}$$

$$G(\tau) = \frac{1}{\beta}\sum_n G(\mathrm{i}\omega_n)e^{-\mathrm{i}\omega_n\tau}\ . \tag{2.92}$$

In lattice system there is a spatial dependence $\alpha = \mathbf{R}$ and due to translational invariance, G only depends on $\mathbf{R}_1 - \mathbf{R}_2$). This means one can transform between real-space and crystal momentum representation as

$$G(\mathbf{k}) = \sum_i G(\mathbf{R}_i)e^{\mathrm{i}\mathbf{k}\mathbf{R}_i} \tag{2.93}$$

$$G(\mathbf{r}) = \frac{1}{N_\mathbf{k}}\sum_\mathbf{k} G(\mathbf{k})e^{-\mathrm{i}\mathbf{k}\mathbf{r}}\ , \tag{2.94}$$

both in τ and Matsubara frequency space.

Matsubara Green's function make calculations computationally easier, but do not give information on experimental observables. This can be done by extending the description to real frequencies ω by analytic continuation [5]

$$G^R(\omega + \mathrm{i}\eta) = G(\mathrm{i}\omega_n \to \omega + \mathrm{i}\eta) \ , \tag{2.95}$$

where the $\eta > 0$ is an infinitesimal part. On real frequencies, the retarded Green's function G^R connects to experimentally measurable quantities, such as the spectral function

$$A(\omega, \mathbf{k}) = -\frac{1}{\pi}\Im(G(\omega + \mathrm{i}\eta, \mathbf{k})) \ , \tag{2.96}$$

describing the excitation spectrum of the system being measured.

Dyson Equation

A non-interacting system with dispersion $\epsilon_{\mathbf{k}}$ can be described by the free Green's function

$$G_0(\mathrm{i}\omega_n, \mathbf{k}) = [\mathrm{i}\omega_n - \epsilon_{\mathbf{k}}]^{(-1)} \tag{2.97}$$

The feedback of the environment on propagation of the particle is encoded in an object called the self-energy $\Sigma(\mathrm{i}\omega_n, \mathbf{k})$. The interacting and non-interacting Green's function are connected by the Dyson equation

$$G = G_0 + G_0 \Sigma G \ . \tag{2.98}$$

The solution to the Dyson equation can formally be written as

$$G(\mathrm{i}\omega_n, \mathbf{k}) = [G_0(\mathrm{i}\omega_n, \mathbf{k}) - \Sigma(\mathbf{k}, \mathrm{i}\omega_n)]^{-1} \ . \tag{2.99}$$

The real part of $\Sigma(\mathbf{k}, \mathrm{i}\omega_n)$ describes renormalization of energy levels and the imaginary part describes the finite lifetime of quasiparticles.

The self-energy enables a systematic inclusion of interaction effects and approximations given certain system restraints. In DMFT, the self-energy is taken to be purely local, which is exact in the limit of infinite dimension, but it can still capture effects which depend significantly on local dynamic correlations in low-dimensional system.

Mapping to Impurity Model and DMFT Self-Consistency Loop

The central idea of DMFT is to map the full lattice problem onto a problem of a single impurity of the form

$$H_{\mathrm{IM}} = H_{\mathrm{imp}} + H_{\mathrm{bath}} + H_{\mathrm{hyb}} \tag{2.100}$$

with the terms

$$H_{\mathrm{imp}} = \sum_{\alpha\sigma} \epsilon_{d,\alpha} d^\dagger_{\alpha\sigma} d_{\alpha\sigma} + \sum_{\alpha} U_\alpha n_{d,\alpha\uparrow} n_{d,\alpha\downarrow} \tag{2.101}$$

$$H_{\mathrm{bath}} = \sum_{\mathbf{k},n\sigma} \epsilon_{\mathbf{k},n} c^\dagger_{\mathbf{k}n\sigma} c_{\mathbf{k}n\sigma} \tag{2.102}$$

$$H_{\mathrm{hyb}} = \sum_{\mathbf{k},\alpha n\sigma} V_{\mathbf{k},\alpha n} d^\dagger_{\alpha\sigma} c_{\mathbf{k}n\sigma} + V^*_{\mathbf{k},n\alpha} c^\dagger_{\mathbf{k}n\sigma} d_{\alpha\sigma} \tag{2.103}$$

Here, d are the operators for the impurity site and c are the operators for the bath, which is characterized by the energy levels $\epsilon_{\mathbf{k},n}$ and hybridization to the impurity orbitals $V_{\mathbf{k},\alpha n}$.

Using the path-integral formalism, the bath degrees of freedom can be integrated out [36]:

$$S_{\mathrm{imp}} = -\int_0^\beta \mathrm{d}\tau\, \mathrm{d}\tau' \sum_{\alpha\beta,\sigma} d^*_{\alpha\sigma}(\tau) [G^{-1}_{\mathrm{imp},0}]_{\alpha\beta}(\tau - \tau') d_{\beta\sigma}(\tau') \tag{2.104}$$

$$+ \int_0^\beta \mathrm{d}\tau \sum_{\alpha} U_\alpha n_{d,\alpha,\uparrow} n_{d,\alpha,\downarrow} \tag{2.105}$$

with the non-interacting impurity Green's funcion $G_{\mathrm{imp},0}$, given by

$$[G_{\mathrm{imp},0}]_{\alpha,\beta} = \left[\mathrm{i}\omega_n - \epsilon_{d,\alpha} - \sum_{\mathbf{k}} \frac{V^*_{\mathbf{k},\alpha n} V_{\mathbf{k},n\beta}}{\mathrm{i}\omega_n - \epsilon_{\mathbf{k},n}} \right] \tag{2.106}$$

The approximation of DMFT lies in the fact that the self-energy of the impurity model $\Sigma_{\mathrm{imp}}(\mathrm{i}\omega_n)$ is purely local, where the lattice self-energy $\Sigma_{\mathrm{lat}}(\mathrm{i}\omega_n, \mathbf{k})$ carries a $\mathbf{k}$-dependence. As shown in the illustration fig. 2.3, these two quantities are set equal to go from the impurity to the lattice model:

$$\Sigma_{\mathrm{lat}}(\mathrm{i}\omega_n, \mathbf{k}) \approx \Sigma_{\mathrm{imp}}(\mathrm{i}\omega_n) =: \Sigma(\mathrm{i}\omega_n)\ . \tag{2.107}$$

Using this, the local lattice Greens function is obtained by summing over the **k**-dependence:

$$G_{\mathrm{loc}}(\mathrm{i}\omega_n) = \frac{1}{N_k}\sum_{\mathbf{k}}[\mathrm{i}\omega_n - h(\mathbf{k}) - \Sigma(\mathrm{i}\omega_n)]^{-1} \stackrel{!}{=} G_{\mathrm{imp}}(\mathrm{i}\omega_n)\ . \tag{2.108}$$

By demanding that this is equal to the impurity Green's function G_{imp}, the mapping to the impurity model is defined. Using the Dyson equation, the non-interacting Greens function for the impurity problem can be calculated as

$$G_{\mathrm{imp},0}(\mathrm{i}\omega_n) = [G^{-1}_{\mathrm{loc}}(\mathrm{i}\omega_n) + \Sigma(\mathrm{i}\omega_n)]^{-1}\ . \tag{2.109}$$

This sets up an impurity model which can be solved by computational means.

Given a solution to the impurity problem with has been found, this interacting Green's function $G_{\mathrm{imp}}(\mathrm{i}\omega_n)$ can be used to calculate the self-energy via

$$\Sigma(\mathrm{i}\omega_n) = G^{-1}_{\mathrm{imp},0}(\mathrm{i}\omega_n) - G^{-1}_{\mathrm{imp}}(\mathrm{i}\omega_n)\ . \tag{2.110}$$

The DMFT self-consistency loop as shown in fig. 2.3 consists of the following steps:

1. Choose an initial self-energy Σ, for example $\Sigma = 0$.
2. Use eq. (2.108) to calculate $G_{\mathrm{loc}}(\mathrm{i}\omega_n)$.
3. Calculate the non-interacting impurity Green's function from eq. (2.109).
4. Solve the interacting impurity model, obtaining $G_{\mathrm{imp}}(\mathrm{i}\omega_n)$.
5. Calculate a new self-energy $\Sigma(\mathrm{i}\omega_n)$ via eq. (2.110).
6. Check convergence of the self-energy (or alternatively via the condition $G_{\mathrm{loc}}(\mathrm{i}\omega_n) = G_{\mathrm{imp}}(\mathrm{i}\omega_n)$). Otherwise, use this self-energy as a new input in step 2.

Step 4, solving the impurity model is the computationally hardest step in the DMFT loop and many different solver methods have been developed over the years with differing use cases, accuracy and numerical demands.

The TRIQS toolkit [37] implements methods to work with Green's functions, using different impurity solvers to enable efficient development of DMFT methods. For the calculations in this thesis, Exact Diagonalization (ED) as

implemented in the EDIpack library [38] has been used. It was made available to TRIQS via a compatibility layer by I. Krivenko and L. Crippa [39].

The idea of ED as introduced by Caffarel and Krauth [40] is to represent the bath with a finite number of discrete bath sites N_b. This means the Hamiltonian for the impurity model is adjusted to

$$H_{\text{bath}} = \sum_{\substack{k\in\{1,\dots,N_b\}\\ n\sigma}} \epsilon_{k,n} c^\dagger_{kn\sigma} c_{kn\sigma} \tag{2.111}$$

$$H_{\text{hyb}} = \sum_{\substack{k\in\{1,\dots,N_b\}\\ \alpha n\sigma}} V_{k,\alpha n} d^\dagger_{\alpha\sigma} c_{kn\sigma} + V_{k,n\alpha} c^\dagger_{kn\sigma} d_{\alpha\sigma} \tag{2.112}$$

In ED, one needs to fit the bath parameters $\{\epsilon_k, V_k\}$ to optimally represent the lattice system, i.e. find the best fit to approximate the hybridization function $\Delta(\mathrm{i}\omega_n)$ of the impurity model by the discrete hybridization function

$$\Delta_{\{\epsilon_k,V_k\}}(\mathrm{i}\omega_n) = \sum_{k=1}^{N_b} \frac{|V_k|^2}{\mathrm{i}\omega_n - \epsilon_k} \tag{2.113}$$

containing only a finite amount of poles. This is implemented in EDIpack.

Nambu-Gorkov Green's Functions

To describe superconductivity in the Green's function formalism, one introduces the Nambu-Gor'kov formalism [36]. Using the Nambu spinors as in eq. (2.59)

$$\Psi_{\mathbf{k},\mathbf{q},\alpha} = \begin{pmatrix} c_{\mathbf{k}\alpha\uparrow} & c^\dagger_{\mathbf{q}-\mathbf{k}\alpha\downarrow} \end{pmatrix}^T , \tag{2.114}$$

the Green's functions become 2×2 matrices in Nambu space

$$[\mathcal{G}_{\mathbf{q}}(\tau,\mathbf{k})]_{\alpha\gamma} = -\langle T_\tau \Psi_{\mathbf{k},\mathbf{q},\alpha} \Psi^\dagger_{\mathbf{k},\mathbf{q},\gamma}\rangle \tag{2.115}$$

$$= \begin{pmatrix} -\langle T_\tau c_{\mathbf{k},\alpha,\uparrow} c^\dagger_{\mathbf{k},\gamma,\uparrow}\rangle & -\langle T_\tau c_{\mathbf{k},\alpha,\uparrow} c_{\mathbf{q}-\mathbf{k},\gamma,\downarrow}\rangle \\ -\langle T_\tau c^\dagger_{\mathbf{q}-\mathbf{k},\alpha,\downarrow} c^\dagger_{\mathbf{k},\gamma,\uparrow}\rangle & -\langle T_\tau c_{\mathbf{q}-\mathbf{k},\alpha,\downarrow} c^\dagger_{\mathbf{q}-\mathbf{k},\gamma,\downarrow}\rangle \end{pmatrix} \tag{2.116}$$

$$= \begin{pmatrix} [\mathcal{G}^{\downarrow\downarrow}_{\mathbf{q}}(\tau,\mathbf{k})]_{\alpha\gamma} & [\mathcal{G}^{\uparrow\downarrow}_{\mathbf{q}}(\tau,\mathbf{k})]_{\alpha\gamma} \\ [\mathcal{G}^{\downarrow\downarrow}_{\mathbf{q}}(\tau,\mathbf{k})]_{\alpha\gamma} & [\mathcal{G}^{\uparrow\downarrow}_{\mathbf{q}}(\tau,\mathbf{k})]_{\alpha\gamma} \end{pmatrix} . \tag{2.117}$$

Due to the definition of the Nambu spinors with $\mathbf{q}$ only appearing in the spin-down sector, only $\mathcal{G}^{\downarrow\downarrow}$ carries the $\mathbf{q}$-dependence. The superconducting state is

marked by the fact that the so-called anomalous Green's functions $\mathcal{G}^{\uparrow\downarrow}, \mathcal{G}^{\downarrow\uparrow}$ are non-zero. On Matsubara frequencies, the Nambu-Gor'kov Green's functions is set up via

$$[\mathcal{G}_{\mathbf{q}}(\mathrm{i}\omega_n, \mathbf{k})]^{-1} \tag{2.118}$$
$$= \begin{pmatrix} (\mathrm{i}\omega_n + \mu) - h(\mathbf{k}) - \Sigma^N(\mathrm{i}\omega_n) & -\Sigma^{\mathrm{AN}}(\mathrm{i}\omega_n) \\ -\Sigma^{\mathrm{AN}}(\mathrm{i}\omega_n) & (\mathrm{i}\omega_n - \mu) + h(-\mathbf{k} + \mathbf{q}) + (\Sigma^N)^*(\mathrm{i}\omega_n) \end{pmatrix}$$

with the self-energy now being composed of a normal and anomalous part:

$$\mathcal{S}(\mathrm{i}\omega_n) = \begin{pmatrix} \Sigma^N(\mathrm{i}\omega_n) & \Sigma^{\mathrm{AN}}(\mathrm{i}\omega_n) \\ \Sigma^{\mathrm{AN}}(\mathrm{i}\omega_n) & -(\Sigma^N)^*(\mathrm{i}\omega_n) \end{pmatrix} \tag{2.119}$$

The self-consistency cycle of DMFT introduced in the section above can equivalently be defined in Nambu space, replacing eqs. (2.108) to (2.110):

$$\begin{cases} \mathcal{G}_{\mathrm{loc}}(\mathrm{i}\omega_n) = \frac{1}{N_k} \sum_{\mathbf{k}} \mathcal{G}(\mathrm{i}\omega_n, \mathbf{k}) \\ \mathcal{G}_{\mathrm{imp},0} = [\mathcal{G}_{\mathrm{loc}}^{-1}(\mathrm{i}\omega_n) + \mathcal{S}(\mathrm{i}\omega_n)]^{-1} \\ \mathcal{S}(\mathrm{i}\omega_n) = \mathcal{G}_{\mathrm{imp},0}^{-1}(\mathrm{i}\omega_n) - \mathcal{G}_{\mathrm{imp}}^{-1}(\mathrm{i}\omega_n) \end{cases} \tag{2.120}$$

2.4 Quantum Geometry

An emerging topic in condensed matter physics is the fact that the geometric properties of the free electron ground state have influence on many (quantum) material properties [10, 41]. The first example of this was the 1980 discovery of the Integer quantum Hall effect [42]. This was explained by Thouless et al. as being a consequence of the unique topology of the electronic ground state which is encoded by the Chern number C [43]. The Chern number is an integer that is the result of the integration of the Berry curvature over the Brillouin zone. The Berry curvature describes the change of the eigenstate's phase as the momentum $\mathbf{k}$ is varied and it is part of the quantum geometry of a material, the geometric structure in the space of quantum states when these states depend on a continuous parameter (lattice momentum $\mathbf{k}$ for solids).

The concept of quantum geometry was first formulated in 1980 by Provost and Vallee [44]. The starting point is a parameter dependent Hamiltonian $\{H(\lambda)\}$ with a smooth dependence on a parameter $\lambda = (\lambda_1, \lambda_2, ...) \in \mathcal{M}$ ($\mathcal{M}$ is

called the base manifold). The Hamiltonian acts on a parametrized Hilbert space $\mathcal{H}(\lambda)$ with eigenenergies $E_n(\lambda)$ and eigenstates $|\phi_n(\lambda)\rangle$. A system state $|\psi(\lambda)\rangle$ is a linear combination of $|\psi_n(\lambda)\rangle$ at every point in $\mathcal{M}$. On infinitesimal variation of the parameter $\mathrm{d}\lambda$, the distance in the space of quantum states is

$$\mathrm{d}s^2 = \||\psi(\lambda + \mathrm{d}\lambda) - \psi(\lambda)\|^2 = \langle \delta\psi | \, \delta\psi \rangle \tag{2.121}$$

$$= \langle \partial_\mu \psi | \, \partial_\nu \psi \rangle \, \mathrm{d}\lambda^\mu \, \mathrm{d}\lambda^\nu = (\gamma_{\mu\nu} + \mathrm{i}\sigma_{\mu\nu}) \, \mathrm{d}\lambda^\mu \, \mathrm{d}\lambda^\nu \, . \tag{2.122}$$

The imaginary part $\sigma_{\mu\nu}$ is the Berry curvature mentioned above. The real part $\gamma_{\mu\nu}$ is not gauge invariant, so in order to have a meaningful notion of a metric one needs to define the gauge invariant quantity

$$g_{\mu\nu} \coloneqq \gamma_{\mu\nu} - \beta_\mu \beta_\nu \, . \tag{2.123}$$

where $\beta_\mu = \mathrm{i} \langle \partial_\mu \psi | \psi \rangle$ is the Berry connection, which is purely real. For simplicity, one defines the quantum geometric tensor:

$$Q_{\mu\nu}(\lambda) \coloneqq \langle \partial_\mu \psi(\lambda) | \, \partial_\nu \psi(\lambda) \rangle - \langle \partial_\mu \psi(\lambda) | \psi(\lambda) \rangle \langle \psi(\lambda) | \, \partial_\nu \psi(\lambda) \rangle \tag{2.124}$$

where now

$$g_{\mu\nu} = \mathrm{Re}\, Q_{\mu\nu}, \; \sigma_{\mu\nu} = \Im Q_{\mu\nu} \, . \tag{2.125}$$

In numerical calculations, the phases of neighboring states are random, so the derivatives of states in the quantum geometric tensor does not give definitive results. Instead, when the system is adiabatic, i.e. the system is restricted to a subspace $\mathcal{H}_{E_0}(\lambda)$ for an instantaneous eigenvalue of Hamiltonian

$$H(\lambda) \, |\phi_0(\lambda)\rangle = E_0(\lambda) \, |\phi_0(\lambda)\rangle \; , \tag{2.126}$$

one can connect to derivatives of the Hamiltonian. Without loss of generality, one can do consider the ground state $|\phi_0(\lambda)\rangle$, for which the quantum geometric tensor is

$$Q_{\mu\nu}(\lambda) = \langle \partial_\mu \phi_0(\lambda) | \, \partial_\nu \phi_0(\lambda) \rangle - \langle \partial_\mu \phi_0(\lambda) | \phi_0(\lambda) \rangle \langle \phi_0(\lambda) | \, \partial_\nu \phi_0(\lambda) \rangle \tag{2.127}$$

$$= \langle \partial_\mu \phi_0 | \, (\mathbb{1} - |\phi_0\rangle \, |\phi_0\rangle) \, |\partial_\nu \phi_0\rangle \tag{2.128}$$

$$= \sum_{n \neq 0} \langle \partial_\mu \phi_0 | \phi_n \rangle \langle \phi_n | \, \partial_\mu \phi_0 \rangle \tag{2.129}$$

The first step is to calculate the partial derivative for the eigenvalue equation

$$\partial_\mu H\,|\phi_0\rangle + H\,|\partial_\mu \phi_0\rangle = \partial_\mu E_0\,|\phi_0\rangle + E_0\,|\partial_\mu \phi_0\rangle \ . \tag{2.130}$$

Multiplying by $\langle\phi_n|$ (with $n \neq 0$, meaning that $\langle\phi_n|\phi_0\rangle = \delta_{n,0} = 0$) gives:

$$\langle\phi_n|\,\partial_\mu H|\phi_0\rangle + \langle\phi_n|H|\,\partial_\mu\phi_0\rangle = \langle\phi_n|\,\partial_\mu E_0|\phi_0\rangle + E_0\,\langle\phi_n\,\partial_\mu\phi_0\rangle \tag{2.131}$$

$$\langle\phi_n|\,\partial_\mu H|\phi_0\rangle + E_n\,\langle\phi_n|\,\partial_\mu\phi_0\rangle = \partial_\mu E_0\,\langle\phi_n|\phi_0\rangle + E_0\,\langle\phi_n|\,\partial_\mu\phi_0\rangle \tag{2.132}$$

$$\langle\phi_n|\,\partial_\mu H|\phi_0\rangle + E_n\,\langle\phi_n|\,\partial_\mu\phi_0\rangle = E_0\,\langle\phi_n|\,\partial_\mu\phi_0\rangle \ . \tag{2.133}$$

This means that the term $\langle\phi_n|\,\partial_\mu\phi_0\rangle$ can be expressed by the derivative of the Hamiltonian:

$$\langle\phi_n|\,\partial_\mu\phi_0\rangle = \frac{\langle\phi_n|\,\partial_\mu H|\phi_0\rangle}{E_n - E_0} \tag{2.134}$$

This gives the following expression for the quantum geometric tensor:

$$Q_{\mu\nu} = \sum_{n\neq 0} \frac{\langle\phi_0|\,\partial_\mu H|\phi_n\rangle\,\langle\phi_n|\,\partial_\nu H|\phi_0\rangle}{(E_0 - E_n)^2} \tag{2.135}$$

For a non-degenerate Bloch eigenstate $|\psi_n(\mathbf{k})\rangle$ with crystal momentum $\mathbf{k}$ and band index n, the quantum geometric tensor is

$$Q^n_{ij} = \sum_{m\neq n} \frac{\langle\psi_n|\,\partial_{k_i} H(\mathbf{k})|\psi_m\rangle\,\langle\psi_m|\,\partial_{k_j} H(\mathbf{k})|\psi_n\rangle}{(E_m - E_n)^2} \tag{2.136}$$

Quantum Metric and Superfluid Weight

The quantum metric became of interest in the context of flat-band superconductivity. From single-band BCS theory, the superfluid weight depends just on the derivative of the band

$$D_{\mathrm{S},ij} = \frac{e^2}{\hbar^2}\int \frac{\mathrm{d}^d\mathbf{k}}{(2\pi)^d} f(\epsilon(\mathbf{k}))\,\frac{\partial^2\epsilon(\mathbf{k})}{\partial k_i\,\partial k_j} \ , \tag{2.137}$$

which is zero for a flat band. On the other hand, $T_\mathrm{C} \propto e^{-1/n_\mathrm{F}U}$ with the density of states at the fermi level n_F so that for a flat band, the critical temperature is

exponentially enhanced. So even though BCS theory predicts pairing, there is no superconductivity with just the single-band superfluid weight.

Peotta and Törmä showed that in multi-band system, there is an additional contribution to the superfluid weight [9]:

$$D_{\mathrm{S,geom},ij} \propto \mathrm{M}_{ij} \tag{2.138}$$

that can be nonzero even for a flat band. M_{ij} is the quantum metric integrated over the Brillouin zone:

$$\mathrm{M}_{ij} = \sum_{\mathbf{k}} \mathrm{Re}\, Q^n_{ij} \tag{2.139}$$

with the band index of the flat band n.

Make notation coherent with my BCS notation for non-interacting H

This connection is derived only in the completely flat band limit, so Liang et al. developed a general theory in the framework of linear response theory which can be used to distinguish conventional and geometric contribution [20]. The superfluid weight from this approach is:

$$D^S_{\mu\nu} = \sum_{\mathbf{k}} \sum_{m,n,p,q} C^{mn}_{pq} [j_{\mu,\uparrow}(\mathbf{k})]_{mn} [j_{\nu,\downarrow}(-\mathbf{k})]_{qp} \tag{2.140}$$

$$C^{mn}_{pq} = 2 \sum_{i,j} \frac{n(E_i) - n(E_j)}{E_j - E_i} w^*_{+,im} w_{+,jn} w^*_{-,jp} w_{-,iq}\,, \tag{2.141}$$

where the E_i are the eigenvalues of the BdG Hamiltonian, so $i \in \{1, \dots, 2 \cdot f\}$ with the number of bands f. The current operator is

$$[j_{\mu,\sigma}(\mathbf{k})]_{mn} = {}_{\sigma}\langle m| \partial_\mu H_\sigma(\mathbf{k}) |n\rangle_{\sigma}\,, \tag{2.142}$$

with $|m\rangle$ being the eigenvectors of the non-interacting Hamiltonian H, the Bloch functions. The w terms are the elements of the unitary matrix $U_{\mathbf{k}}$ that diagonalizes the BdG Hamiltonian eq. (2.61):

$$U_{\mathbf{k}} = \begin{pmatrix} w_{+,11} & w_{+,21} & \dots & w_{+,2\cdot f1} \\ w_{+,12} & w_{+,22} & \dots & w_{+,2\cdot f2} \\ \vdots & \vdots & \ddots & \vdots \\ w_{+,1f} & w_{+,2f} & \dots & w_{+,2\cdot ff} \\ w_{-,11} & w_{-,21} & \dots & w_{-,2\cdot f1} \\ w_{-,12} & w_{-,22} & \dots & w_{-,2\cdot f2} \\ \vdots & \vdots & \ddots & \vdots \\ w_{-,1f} & w_{-,2f} & \dots & w_{-,2\cdot ff} \end{pmatrix} \tag{2.143}$$

Equation (2.140) splits up into to two parts:

$$D^S_{\mu\nu} = D^S_{\text{conv},\mu\nu} + D^S_{\text{geom},\mu\nu} \tag{2.144}$$

where the geometric term $D^S_{\text{geom},\mu\nu}$ is the term that only depends on the off-diagonal elements of the current operator:

$$D^S_{\text{geom},\mu\nu} = \sum_{\mathbf{k}} \sum_{m\neq n, p\neq q} C^{mn}_{pq} [j_{\mu,\uparrow}(\mathbf{k})]_{mn} [j_{\nu,\downarrow}(-\mathbf{k})]_{qp} \tag{2.145}$$

The formula eq. (2.140) will be used in this thesis to compare with the results from the FMP method.

To understand this connection between the superfluid weight and the quantum metric, the concept of Wannier functions is needed. They are the Fourier transform of the Bloch functions, so while Bloch functions are localized in energy, Wannier functions are localized in space [45]. Wannier functions are used to characterize electronic orbitals in solids, most commonly in the form of maximally localized Wannier functions [46]. They have two important properties: the center of the Wannier function showing the center of the electronic orbital and the spread showing how localized the maximally localized Wannier functions are.

A flat-band system can be described by an effective spin Hamiltonian in which the exchange coupling (and in the superfluid weight) is controlled by the overlap of the Wannier functions [47]. Because the spread of the Wannier functions is bounded from below by the trace of the integrated quantum metric

$$\mathrm{M}_{ij} = \sum_{\mathbf{k}} \mathrm{Re}\, Q^n_{ij} \,, \tag{2.146}$$

this connects the superfluid weight and the quantum metric as in eq. (2.138).

In magic angle twisted bilayer Graphene, one of the prime example for a flat band system supporting superconductivity it has recently been measured that the superfluid weight cannot be explained by the conventional contributions alone and it is instead carried by geometric contributions [48].

Decorated Graphene Model 3

Following the 2018 discovery of superconductivity in twisted bilayer Graphene [49], graphene-based systems gained a renewed interest as a platform for strongly correlated physics. Two methods to engineer strong electron correlations emerged: twisted multilayer systems [48–52] and multilayer systems without twisting, such as Bernal bilayer, ABC or ABCA layered systems [53]. Through different means, electrons in these systems become localized so that interaction effects get more strongly pronounced. Connecting both kind of systems is the strong quantum geometry coming from the Graphene Dirac cones [54], which plays a role in stabilizing superconducting [20, 48] and magnetic order [55, 56].

Witt et al. suggested another platform for strongly correlated physics based on Graphene with the same strong quantum geometry, but higher intrinsic energy scales and thus also higher critical temperatures for strong correlation phenomena [57]. The model is inspired by an earlier experiment [58] of a SiC(0001) substrate with a single layer of Graphene on top and Sn as an intercalant[1] between the substrate and the Graphene layer. The system shows signs of Mott-Hubbard bands, a hallmark of strong correlation physics. Witt et al. suggested that by using different group-IV intercalants (C, Si, Ge, Sn, Pb) between the graphene sheet and the semiconducting SiC(0001) substrate, different distances to the Graphene sheet occur in the ground state. Band structures obtained from Density Functional Theory (DFT) show a relatively flat band at the Fermi level from the intercalant's p_z orbitals hybridized to the Dirac bands of graphene for all intercalants, with the hybridization strength being tuned by the equilibrium distance of the Graphene sheet and the intercalants.

In this thesis I will be treating an elemental model introduced in the work by Witt et al. capturing the essential flat band character of the system. The lattice structure can be seen in fig. 3.1. It consists of the usual hexagonal Graphene lattice, with an additional atom at one of the sublattice sites providing the flat band. Here, the hopping V models the hybridization

[1] An intercalant is an atom or molecule inserted between the layers of layered system.

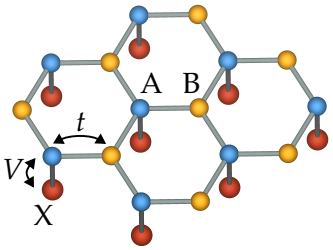

Figure 3.1 – Lattice structure of decorated graphene honeycomb lattice. with impurity X hybridized to sublattice site A. There is only hopping t between sublattices A and B as well as V between X and A atoms. Created using VESTA [59].

This elemental model shows two symmetry distinct Mott states for the small and large V regimes: in the low V regime, the X are responsible for the development of local moments and Mottness occurs at, where in the high V limit, the B atom are responsible. Between these Mott states emerges a metallic state, similar to the topological phase transition of non-interacting bands in the Su-Schrieffer-Heger model [60].

In twisted or untwisted multilayer Graphene systems, the energy scale for the emergence of ordered phases is $O(\text{meV})$, corresponding to temperatures of a few K [61, 62]. In contrast, the energy scale in this decorated Graphene model is set by the hopping t, i.e. $O(\text{eV})$ for Graphene, so that the correlated flat band physics might persist to higher temperatures.

3.1 Lattice Structure

Monolayer graphene forms a honeycomb lattice [63], which is a hexagonal Bravais lattice with a two-atom basis, as can be seen in fig. 3.2a. The primitive lattice vectors of the hexagonal lattice are:

$$\mathbf{a}_1 = \frac{a}{2}\begin{pmatrix} 1 \\ \sqrt{3} \end{pmatrix}, \ \mathbf{a}_2 = \frac{a}{2}\begin{pmatrix} 1 \\ -\sqrt{3} \end{pmatrix} \tag{3.1}$$

with lattice constant $a = \sqrt{3}a_0 \approx 2.46\,\text{Å}$, using the nearest-neighbor distance a_0. The vectors from atom A to the nearest-neighbor atoms B_i $(i = 1, 2, 3,)$ are

$$\delta_{AB,1} = \begin{pmatrix} 0 \\ \frac{a}{\sqrt{3}} \end{pmatrix}, \ \delta_{AB,2} = \begin{pmatrix} \frac{a}{2} \\ -\frac{a}{2\sqrt{3}} \end{pmatrix}, \ \delta_{AB,3} = \begin{pmatrix} -\frac{a}{2} \\ -\frac{a}{2\sqrt{3}} \end{pmatrix} \tag{3.2}$$

(a) (b)

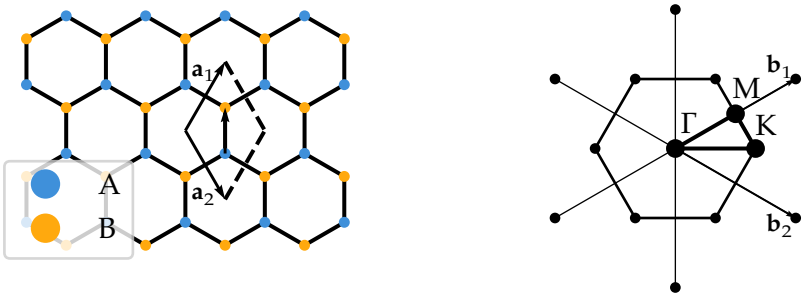

Figure 3.2 – Graphene lattice structure and Brillouin zone. (**a**) Graphene lattice structure with primitive lattice vectors $\mathbf{a}_1$, $\mathbf{a}_2$ and (**b**) Brillouin zone with reciprocal vectors $\mathbf{b}_1$, $\mathbf{b}_2$. Both images created with lattpy [64].

and the vectors from atom B to the nearest-neighbor atoms A_i $(i = 1, 2, 3,)$ are

$$\delta_{BA,1} = \begin{pmatrix} 0 \\ -\frac{a}{\sqrt{3}} \end{pmatrix}, \; \delta_{BA,2} = \begin{pmatrix} -\frac{a}{2} \\ \frac{a}{2\sqrt{3}} \end{pmatrix}, \; \delta_{BA,3} = \begin{pmatrix} \frac{a}{2} \\ \frac{a}{2\sqrt{3}} \end{pmatrix} . \tag{3.3}$$

The primitive reciprocal lattice vectors $\mathbf{b}_1$, $\mathbf{b}_2$ fulfill:

$$\mathbf{a}_1 \cdot \mathbf{b}_1 = \mathbf{a}_2 \cdot \mathbf{b}_2 = 2\pi \tag{3.4}$$

$$\mathbf{a}_1 \cdot \mathbf{b}_2 = \mathbf{a}_2 \cdot \mathbf{b}_1 = 0 \,, \tag{3.5}$$

so that

$$\mathbf{b}_1 = \frac{2\pi}{a} \begin{pmatrix} 1 \\ \frac{1}{\sqrt{3}} \end{pmatrix}, \; \mathbf{b}_2 = \frac{2\pi}{a} \begin{pmatrix} 1 \\ -\frac{1}{\sqrt{3}} \end{pmatrix} . \tag{3.6}$$

The first Brillouin zone of the hexagonal lattice is shown in fig. 3.2b, with the points of high symmetry

$$\Gamma = \begin{pmatrix} 0 \\ 0 \end{pmatrix}, \; \mathrm{M} = \frac{\pi}{a} \begin{pmatrix} 1 \\ \frac{1}{\sqrt{3}} \end{pmatrix}, \; \mathrm{K} = \frac{4\pi}{3a} \begin{pmatrix} 1 \\ 0 \end{pmatrix} . \tag{3.7}$$

The elemental model as shown in fig. 3.1 has the following kinetic terms:

$$H_0 = -t \sum_{\langle ij\rangle,\sigma} c_{i\sigma}^{(\mathrm{A}),\dagger} c_{j\sigma}^{(\mathrm{B})} + V \sum_{i\sigma\sigma'} d_{i\sigma}^{\dagger} c_{i\sigma'}^{(\mathrm{A})} + \mathrm{h.c.} \tag{3.8}$$

with

- d - operators on the X atom
- $c^{(\epsilon)}$ - operators on the graphene sites ($\epsilon = \mathrm{A}, \mathrm{B}$)
- t - nearest neighbor hopping between Graphene sites
- V - hopping between X and Graphene A sites.

Using the Fourier transformation

$$c_{i\alpha\sigma} = \frac{1}{\sqrt{N}} \sum_{\mathbf{k}} e^{\mathrm{i}\mathbf{k}\mathbf{r}_{i\alpha}} c_{\mathbf{k}\alpha\sigma} \,, \tag{3.9}$$

the hopping term becomes

$$-t \sum_{\langle ij\rangle,\sigma} c_{i\sigma}^{(\mathrm{A}),\dagger} c_{j\sigma}^{(\mathrm{B})} \tag{3.10}$$

$$= -t \sum_{i\delta_{\mathrm{AB}}\sigma} c_{i\sigma}^{(\mathrm{A})\dagger} c_{i+\delta_{\mathrm{AB}},\sigma}^{(\mathrm{B})} \tag{3.11}$$

$$= -\frac{t}{N^2} \sum_{i,\sigma} \sum_{\mathbf{k},\mathbf{k}',\delta_{\mathrm{AB}}} \left(e^{-\mathrm{i}\mathbf{k}\mathbf{r}_{i\alpha}} c_{\mathbf{k}\sigma}^{(\mathrm{A})\dagger}\right) \left(e^{\mathrm{i}\mathbf{k}'\mathbf{r}_{i\alpha}+\delta_{AB}} c_{\mathbf{k}'\sigma}^{(B)}\right) \tag{3.12}$$

$$= -\frac{t}{N^2} \sum_{\mathbf{k},\mathbf{k}',\delta_{\mathrm{AB}},\sigma} c_{\mathbf{k}\sigma}^{(\mathrm{A})\dagger} c_{\mathbf{k}'\sigma}^{(\mathrm{B})} e^{\mathrm{i}\mathbf{k}'\delta_{\mathrm{AB}}} e^{\mathrm{i}(\mathbf{k}(\delta_A-\delta_B)+\mathbf{k}'(\delta_A-\delta_B))} \sum_i e^{-\mathrm{i}\mathbf{k}\mathbf{R}_i} e^{\mathrm{i}\mathbf{k}'\mathbf{R}_i} \tag{3.13}$$

$$= -\frac{t}{N^2} \sum_{\mathbf{k},\mathbf{k}',\sigma} c_{\mathbf{k}\sigma}^{(\mathrm{A})\dagger} c_{\mathbf{k}'\sigma}^{(\mathrm{B})} \sum_{\delta_{\mathrm{AB}}} e^{\mathrm{i}\mathbf{k}'\delta_{\mathrm{AB}}} e^{\mathrm{i}(\mathbf{k}(\delta_A-\delta_B)+\mathbf{k}'(\delta_A-\delta_B))} \left(N^2 \delta_{\mathbf{k},\mathbf{k}'}\right) \tag{3.14}$$

$$= -t \sum_{\mathbf{k},\sigma} c_{\mathbf{k}\sigma}^{(\mathrm{A})\dagger} c_{\mathbf{k}\sigma}^{(\mathrm{B})} \sum_{\delta_{\mathrm{AB}}} e^{\mathrm{i}(\mathbf{k}\delta_{AB}+2k_y a)} = \sum_{\mathbf{k},\sigma} f_{\mathbf{k}} c_{\mathbf{k}\sigma}^{(\mathrm{A})\dagger} c_{\mathbf{k}\sigma}^{(\mathrm{B})} \,. \tag{3.15}$$

The factor $f_{\mathbf{k}}$ can be written out explicitly using the nearest-neighbor vectors, for example

$$\mathbf{k} \cdot \delta_{\mathbf{AB},1} = \begin{pmatrix} k_x \\ k_y \end{pmatrix} \cdot \begin{pmatrix} 0 \\ \frac{a}{\sqrt{3}} \end{pmatrix} = \frac{1}{\sqrt{3}} k_y \,. \tag{3.16}$$

This gives:

$$f_{\mathbf{k}} = -t \sum_{\delta_{AB}} e^{\mathrm{i}(\mathbf{k}\delta_{AB} + 2k_y a)} \tag{3.17}$$

$$= -te^{2\mathrm{i}k_y a} \left(e^{\mathrm{i}\frac{a}{\sqrt{3}}k_y} + e^{\mathrm{i}\frac{a}{2\sqrt{3}}(\sqrt{3}k_x - k_y)} + e^{\mathrm{i}\frac{a}{2\sqrt{3}}(-\sqrt{3}k_x - k_y)} \right) \tag{3.18}$$

$$= -te^{2\mathrm{i}k_y a} \left(e^{\mathrm{i}\frac{a}{\sqrt{3}}k_y} + 2e^{-\mathrm{i}\frac{a}{2\sqrt{3}}k_y} \cos\left(\frac{a}{2}k_x\right) \right) . \tag{3.19}$$

Using the fact that $\delta_{\mathrm{BA},i} = -\delta_{\mathrm{AB},i}$, it follows

$$-t \sum_{\delta_{BA}} e^{\mathrm{i}\mathbf{k}\delta_{BA}} = -t \sum_{\delta_{AB}} e^{-\mathrm{i}\mathbf{k}\delta_{AB}} = \left(-t \sum_{\delta_{AB}} e^{\mathrm{i}\mathbf{k}\delta_{AB}} \right)^* = f_{\mathbf{k}}^* , \tag{3.20}$$

which then gives

$$H_0 = \sum_{\mathbf{k},\sigma} C_{\mathbf{k}\sigma}^\dagger \begin{pmatrix} 0 & f_{\mathbf{k}} & V \\ f_{\mathbf{k}}^* & 0 & 0 \\ V & 0 & 0 \end{pmatrix} C_{\mathbf{k}\sigma} \tag{3.21}$$

$$C_{\mathbf{k}\sigma} = \begin{pmatrix} c_{\mathbf{k}\sigma}^{A,\dagger} & c_{\mathbf{k}\sigma}^{B,\dagger} & d_{\mathbf{k}\sigma}^\dagger \end{pmatrix}^T \tag{3.22}$$

For the Hamiltonian in eq. (3.8) at half-filling, there always is a zero energy eigenstate with a gap separating the other bands from the zero energy band for any finite value, as shown in fig. 3.3. For $V \to \infty$, the eigenstate is $\begin{pmatrix} 0 & 1 & 0 \end{pmatrix}^T$ meaning it is completely localized at the atoms of the non-decorated sublattice B. The maximally localized Wannier function associated with this state is centered and completely peaked in the B sublattice. In the opposite case of $V \to 0^+$, the eigenstate is $\begin{pmatrix} 0 & 0^+ & f_{\mathbf{k}}/f_{\mathbf{k}} \end{pmatrix}^T$ except for the nodal points where $f_{\mathbf{k}} = 0$. This means that the spectral weight of the flat band is located at the X atoms.

The orbital weight of a Bloch state $|\psi_n(\mathbf{k})\rangle$ corresponding to a band n can be calculated using

$$|w_{\mathbf{k}m}^n|^2 = |\langle \Psi_n(\mathbf{k}) | m \rangle|^2 \tag{3.23}$$

where $m \in \{\mathrm{Gr_A}, \mathrm{Gr_B}, \mathrm{X}\}$ marks the orbital:

$$|\mathrm{Gr_A}\rangle = \begin{pmatrix} 1 & 0 & 0 \end{pmatrix}^T , \; |\mathrm{Gr_B}\rangle = \begin{pmatrix} 0 & 1 & 0 \end{pmatrix}^T , \; |\mathrm{X}\rangle = \begin{pmatrix} 0 & 0 & 1 \end{pmatrix}^T . \tag{3.24}$$

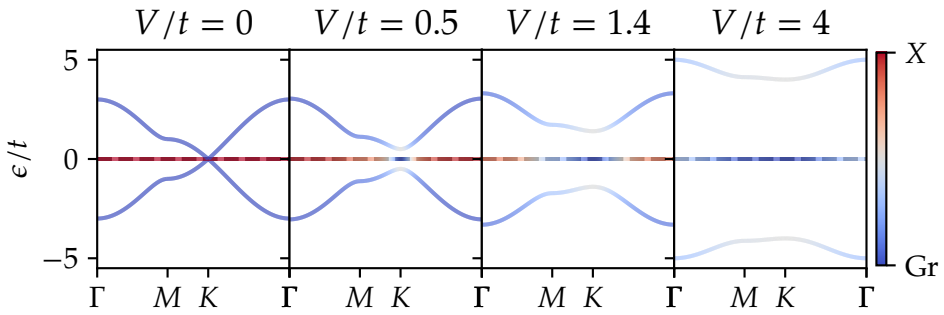

Figure 3.3 – Decorated Graphene band structure. The orbital weight $W_{\mathbf{k}}$ is marked in color, showing how the flat band switches over from being of X character to being of Gr character when tuning the hybridization V.

The orbital character of the bands in fig. 3.3 is calculated via

$$W_{\mathbf{k}} = w_{\mathbf{k},X} - (w_{\mathbf{k},\mathrm{Gr_A}} + w_{\mathbf{k},\mathrm{Gr_A}}) \,. \tag{3.25}$$

It shows how the flat band switches over from being completely of X character to being of Gr character.

3.2 Quantum Geometry

Between the edge cases of $V \to \infty$ and $V \to 0^+$, there is no gap closure when keeping $V > 0$, which means that the Wannier center must not have moved. Instead, the maxima of the Wannier centers shift to the three neighboring X sites. As already discussed in section 2.4, this behavior of the Wannier spread is dictated by the quantum metric. Figure 3.4 shows how the X-orbital weight of the flat band follows the integrated quantum metric

$$M = \frac{1}{N_{\mathbf{k}}} \sum_{\mathbf{k}} g_{xx}(\mathbf{k}) + g_{yy}(\mathbf{k}) \tag{3.26}$$

being finite for low V and then going to 0 for large V. This mean that following section 2.4, the model does not support superconductivity for high V because there is no geometric contribution to the superfluid weight at the flat band. For low V there will be a geometric contribution, so superconductivity can be expected in that parameter regime. The structure of localized orbitals hybridizing

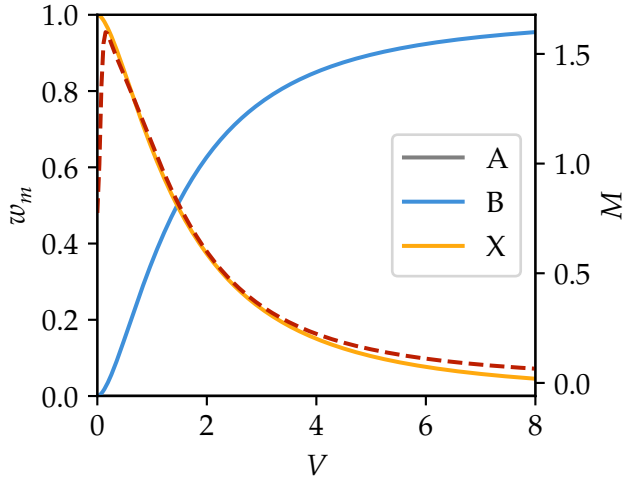

Figure 3.4 – Orbital weight of the flat band and integrated quantum metric. The orbital weight is calculated as $w_m = \sum_{\mathbf{k}} |w_{\mathbf{k}m}|^2$ ($m \in \{\mathrm{Gr_A}, \mathrm{Gr_B}, \mathrm{X}\}$) and the integrated quantum metric M is marked as a dotted line.

with Dirac states is similar to other strongly correlated Graphene systems, such as in the heavy Fermion description of magic angle twisted bilayer Graphene [65].

Application of the Finite-Momentum Pairing Method

4

5 Conclusion

Summary

Outlook

Bibliography

[1] L. N. Cooper and D. Feldman. *BCS: 50 Years*. WORLD SCIENTIFIC, Nov. 2010. ISBN: 978-981-4304-64-1. DOI: 10.1142/7728 (cit. on p. ii).

[2] B. Keimer and J. E. Moore. "The Physics of Quantum Materials". In: *Nature Physics* 13.11 (Nov. 2017), pp. 1045–1055. ISSN: 1745-2481. DOI: 10.1038/nphys4302 (cit. on p. 2).

[3] P. Coleman. *Introduction to Many-Body Physics*. Cambridge University Press, Nov. 2015. ISBN: 978-0-521-86488-6. DOI: 10.1017/CBO9781139020916 (cit. on pp. 2, 12, 19).

[4] M. Tinkham. *Introduction to Superconductivity*. 2. ed. International Series in Pure and Applied Physics. New York: McGraw-Hill, 1996. 454 pp. ISBN: 978-0-07-064878-4 (cit. on pp. 2, 10, 12).

[5] H. Bruus and K. Flensberg. *Many-Body Quantum Theory in Condensed Matter Physics: An Introduction*. Oxford Graduate Texts. Oxford, New York: Oxford University Press, Nov. 11, 2004. 466 pp. ISBN: 978-0-19-856633-5 (cit. on pp. 2, 19, 21).

[6] A. I. Larkin and A. A. Varlamov. *Theory of Fluctuations in Superconductors*. Oxford Science Publications 127. Oxford Oxford: Clarendon Press Oxford University Press, 2005. ISBN: 978-0-19-852815-9 (cit. on p. 2).

[7] K. H. Bennemann and J. B. Ketterson, eds. *Superconductivity*. Berlin, Heidelberg: Springer Berlin Heidelberg, 2008. ISBN: 978-3-540-73252-5. DOI: 10.1007/978-3-540-73253-2 (cit. on p. 2).

[8] N. Witt et al. "Bypassing the Lattice BCS–BEC Crossover in Strongly Correlated Superconductors through Multiorbital Physics". In: *npj Quantum Materials* 9.1 (Dec. 10, 2024), pp. 1–10. ISSN: 2397-4648. DOI: 10.1038/s41535-024-00706-7 (cit. on pp. 2, 9).

[9] S. Peotta and P. Törmä. "Superfluidity in Topologically Nontrivial Flat Bands". In: *Nature Communications* 6.1 (Nov. 20, 2015), p. 8944. ISSN: 2041-1723. DOI: 10.1038/ncomms9944 (cit. on pp. 2, 10, 15, 28).

[10] J. Yu et al. *Quantum Geometry in Quantum Materials*. Dec. 30, 2024. DOI: 10.48550/arXiv.2501.00098. Pre-published (cit. on pp. 2, 25).

[11] E. Noether. "Invariante Variationsprobleme". In: *Nachrichten von der Gesellschaft der Wissenschaften zu Göttingen, Mathematisch-Physikalische Klasse* 1918 (1918), pp. 235–257. URL: https://eudml.org/doc/59024 (visited on 12/10/2024) (cit. on p. 3).

[12] L. D. Landau. "On the Theory of Phase Transitions". In: *Zhurnal Eksperimental'noi i Teoreticheskoi Fiziki* 7 (1937). Ed. by D. ter Haar, pp. 19–32. DOI: 10.1016/B978-0-08-010586-4.50034-1 (cit. on p. 3).

[13] V. L. Ginzburg and L. D. Landau. "On the Theory of Superconductivity". In: *Zhurnal Eksperimental'noi i Teoreticheskoi Fiziki* 20 (1950). Ed. by D. ter Haar, pp. 1064–1082. DOI: 10.1016/b978-0-08-010586-4.50078-x (cit. on pp. 3, 5).

[14] A. Q. Chen et al. "Finite Momentum Cooper Pairing in Three-Dimensional Topological Insulator Josephson Junctions". In: *Nature Communications* 9.1 (Aug. 28, 2018), p. 3478. ISSN: 2041-1723. DOI: 10.1038/s41467-018-05993-w (cit. on p. 9).

[15] P. Wan et al. "Orbital Fulde–Ferrell–Larkin–Ovchinnikov State in an Ising Superconductor". In: *Nature* 619.7968 (July 2023), pp. 46–51. ISSN: 1476-4687. DOI: 10.1038/s41586-023-05967-z (cit. on p. 9).

[16] N. F. Q. Yuan and L. Fu. "Supercurrent Diode Effect and Finite-Momentum Superconductors". In: *Proceedings of the National Academy of Sciences* 119.15 (Apr. 12, 2022), e2119548119. DOI: 10.1073/pnas.2119548119 (cit. on p. 9).

[17] J. J. Kinnunen et al. "The Fulde–Ferrell–Larkin–Ovchinnikov State for Ultracold Fermions in Lattice and Harmonic Potentials: A Review". In: *Reports on Progress in Physics* 81.4 (Feb. 2018), p. 046401. ISSN: 0034-4885. DOI: 10.1088/1361-6633/aaa4ad (cit. on pp. 9, 14).

[18] J. Bardeen. "Critical Fields and Currents in Superconductors". In: *Reviews of Modern Physics* 34.4 (Oct. 1, 1962), pp. 667–681. DOI: 10.1103/RevModPhys.34.667 (cit. on p. 10).

[19] K. Xu, P. Cao, and J. R. Heath. "Achieving the Theoretical Depairing Current Limit in Superconducting Nanomesh Films". In: *Nano Letters* 10.10 (Oct. 13, 2010), pp. 4206–4210. ISSN: 1530-6984. DOI: 10.1021/nl102584j (cit. on p. 10).

[20] L. Liang et al. "Band Geometry, Berry Curvature, and Superfluid Weight". In: *Physical Review B* 95.2 (Jan. 27, 2017), p. 024515. DOI: 10.1103/PhysRevB.95.024515 (cit. on pp. 10, 28, 30).

[21] J. Bardeen, L. N. Cooper, and J. R. Schrieffer. "Theory of Superconductivity". In: *Physical Review* 108.5 (Dec. 1, 1957), pp. 1175–1204. DOI: 10.1103/PhysRev.108.1175 (cit. on p. 11).

[22] L. C. Hebel and C. P. Slichter. "Nuclear Relaxation in Superconducting Aluminum". In: *Physical Review* 107.3 (Aug. 1, 1957), pp. 901–902. DOI: 10.1103/PhysRev.107.901 (cit. on p. 12).

[23] L. C. Hebel and C. P. Slichter. "Nuclear Spin Relaxation in Normal and Superconducting Aluminum". In: *Physical Review* 113.6 (Mar. 15, 1959), pp. 1504–1519. DOI: 10.1103/PhysRev.113.1504 (cit. on p. 12).

[24] I. Giaever and K. Megerle. "Study of Superconductors by Electron Tunneling". In: *Physical Review* 122.4 (May 15, 1961), pp. 1101–1111. DOI: 10.1103/PhysRev.122.1101 (cit. on p. 12).

[25] F. London. "A New Conception of Supraconductivity". In: *Nature* 140.3549 (Nov. 1, 1937), pp. 793–796. ISSN: 1476-4687. DOI: 10.1038/140793a0 (cit. on p. 12).

[26] X. Zhou et al. "High-Temperature Superconductivity". In: *Nature Reviews Physics* 3.7 (July 2021), pp. 462–465. ISSN: 2522-5820. DOI: 10.1038/s42254-021-00324-3 (cit. on p. 12).

[27] J. Hubbard and B. H. Flowers. "Electron Correlations in Narrow Energy Bands". In: *Proceedings of the Royal Society of London. Series A. Mathematical and Physical Sciences* 276.1365 (Nov. 26, 1963), pp. 238–257. DOI: 10.1098/rspa.1963.0204 (cit. on p. 12).

[28] J. Kanamori. "Electron Correlation and Ferromagnetism of Transition Metals". In: *Progress of Theoretical Physics* 30.3 (Sept. 1, 1963), pp. 275–289. ISSN: 0033-068X. DOI: 10.1143/PTP.30.275 (cit. on p. 12).

[29] M. C. Gutzwiller. "Effect of Correlation on the Ferromagnetism of Transition Metals". In: *Physical Review Letters* 10.5 (Mar. 1, 1963), pp. 159–162. DOI: 10.1103/PhysRevLett.10.159 (cit. on p. 12).

[30] F. C. Zhang and T. M. Rice. "Effective Hamiltonian for the Superconducting Cu Oxides". In: *Physical Review B* 37.7 (Mar. 1, 1988), pp. 3759–3761. DOI: 10.1103/PhysRevB.37.3759 (cit. on p. 12).

[31] M. Qin et al. "The Hubbard Model: A Computational Perspective". In: *Annual Review of Condensed Matter Physics* 13 (Volume 13, 2022 Mar. 10, 2022), pp. 275–302. ISSN: 1947-5454, 1947-5462. DOI: 10.1146/annurev-conmatphys-090921-033948 (cit. on p. 13).

[32] R. Micnas, J. Ranninger, and S. Robaszkiewicz. "Superconductivity in Narrow-Band Systems with Local Nonretarded Attractive Interactions". In: *Reviews of Modern Physics* 62.1 (Jan. 1, 1990), pp. 113–171. DOI: 10.1103/RevModPhys.62.113 (cit. on p. 13).

[33] D. B. McWhan, T. M. Rice, and J. P. Remeika. "Mott Transition in Cr-Doped V2O3". In: *Physical Review Letters* 23.24 (Dec. 15, 1969), pp. 1384–1387. ISSN: 0031-9007. DOI: 10.1103/PhysRevLett.23.1384 (cit. on p. 19).

[34] M. J. Rozenberg, G. Kotliar, and X. Y. Zhang. "Mott-Hubbard Transition in Infinite Dimensions. II". In: *Physical Review B* 49.15 (Apr. 15, 1994), pp. 10181–10193. ISSN: 0163-1829, 1095-3795. DOI: 10.1103/PhysRevB.49.10181 (cit. on p. 19).

[35] E. Pavarini et al., eds. *Dynamical Mean-Field Theory of Correlated Electrons*. Schriften Des Forschungszentrums Jülich Reihe Modeling and Simulation Band/volume 12. Jülich: Forschungszentrum Jülich, Zentralbibliothek, Verlag, 2022. 1 p. ISBN: 978-3-95806-619-9 (cit. on p. 19).

[36] A. Georges et al. "Dynamical Mean-Field Theory of Strongly Correlated Fermion Systems and the Limit of Infinite Dimensions". In: *Reviews of Modern Physics* 68.1 (Jan. 1, 1996), pp. 13–125. DOI: 10.1103/RevModPhys.68.13 (cit. on pp. 19, 22, 24).

[37] O. Parcollet et al. "TRIQS: A Toolbox for Research on Interacting Quantum Systems". In: *Computer Physics Communications* 196 (Nov. 1, 2015), pp. 398–415. ISSN: 0010-4655. DOI: 10.1016/j.cpc.2015.04.023 (cit. on p. 23).

[38] A. Amaricci et al. "EDIpack: A Parallel Exact Diagonalization Package for Quantum Impurity Problems". In: *Computer Physics Communications* 273 (Apr. 1, 2022), p. 108261. ISSN: 0010-4655. DOI: 10.1016/j.cpc.2021.108261 (cit. on p. 24).

[39] I. Krivenko. *Krivenko/Edipack2triqs*. Mar. 10, 2025. URL: https://github.com/krivenko/edipack2triqs (visited on 03/11/2025) (cit. on p. 24).

[40] M. Caffarel and W. Krauth. "Exact Diagonalization Approach to Correlated Fermions in Infinite Dimensions: Mott Transition and Superconductivity". In: *Physical Review Letters* 72.10 (Mar. 7, 1994), pp. 1545–1548. DOI: 10.1103/PhysRevLett.72.1545 (cit. on p. 24).

[41] R. Cheng. *Quantum Geometric Tensor (Fubini-Study Metric) in Simple Quantum System: A Pedagogical Introduction*. Apr. 5, 2013. DOI: 10.48550/arXiv.1012.1337. Pre-published (cit. on p. 25).

[42] K. v. Klitzing, G. Dorda, and M. Pepper. "New Method for High-Accuracy Determination of the Fine-Structure Constant Based on Quantized Hall Resistance". In: *Physical Review Letters* 45.6 (Aug. 11, 1980), pp. 494–497. DOI: 10.1103/PhysRevLett.45.494 (cit. on p. 25).

[43] D. J. Thouless et al. "Quantized Hall Conductance in a Two-Dimensional Periodic Potential". In: *Physical Review Letters* 49.6 (Aug. 9, 1982), pp. 405–408. DOI: 10.1103/PhysRevLett.49.405 (cit. on p. 25).

[44] J. P. Provost and G. Vallee. "Riemannian Structure on Manifolds of Quantum States". In: *Communications in Mathematical Physics* 76.3 (Sept. 1, 1980), pp. 289–301. ISSN: 1432-0916. DOI: 10.1007/BF02193559 (cit. on p. 25).

[45] N. Marzari et al. “Maximally Localized Wannier Functions: Theory and Applications”. In: *Reviews of Modern Physics* 84.4 (Oct. 10, 2012), pp. 1419–1475. DOI: 10.1103/RevModPhys.84.1419 (cit. on p. 29).

[46] N. Marzari and D. Vanderbilt. “Maximally Localized Generalized Wannier Functions for Composite Energy Bands”. In: *Physical Review B* 56.20 (Nov. 15, 1997), pp. 12847–12865. DOI: 10.1103/PhysRevB.56.12847 (cit. on p. 29).

[47] M. Tovmasyan et al. “Effective Theory and Emergent $\text{SU}(2)$ Symmetry in the Flat Bands of Attractive Hubbard Models”. In: *Physical Review B* 94.24 (Dec. 30, 2016), p. 245149. DOI: 10.1103/PhysRevB.94.245149 (cit. on p. 29).

[48] M. Tanaka et al. “Superfluid Stiffness of Magic-Angle Twisted Bilayer Graphene”. In: *Nature* 638.8049 (Feb. 2025), pp. 99–105. ISSN: 1476-4687. DOI: 10.1038/s41586-024-08494-7 (cit. on pp. 29, 30).

[49] Y. Cao et al. “Unconventional Superconductivity in Magic-Angle Graphene Superlattices”. In: *Nature* 556.7699 (Apr. 2018), pp. 43–50. ISSN: 1476-4687. DOI: 10.1038/nature26160 (cit. on p. 30).

[50] P. Törmä, S. Peotta, and B. A. Bernevig. “Superconductivity, Superfluidity and Quantum Geometry in Twisted Multilayer Systems”. In: *Nature Reviews Physics* 4.8 (Aug. 2022), pp. 528–542. ISSN: 2522-5820. DOI: 10.1038/s42254-022-00466-y (cit. on p. 30).

[51] E. Y. Andrei and A. H. MacDonald. “Graphene Bilayers with a Twist”. In: *Nature Materials* 19.12 (Dec. 2020), pp. 1265–1275. ISSN: 1476-4660. DOI: 10.1038/s41563-020-00840-0 (cit. on p. 30).

[52] F. Xie et al. “Topology-Bounded Superfluid Weight in Twisted Bilayer Graphene”. In: *Physical Review Letters* 124.16 (Apr. 24, 2020), p. 167002. DOI: 10.1103/PhysRevLett.124.167002 (cit. on p. 30).

[53] P. A. Pantaleón et al. “Superconductivity and Correlated Phases in Non-Twisted Bilayer and Trilayer Graphene”. In: *Nature Reviews Physics* 5.5 (May 2023), pp. 304–315. ISSN: 2522-5820. DOI: 10.1038/s42254-023-00575-2 (cit. on p. 30).

[54] T. Wehling, A. Black-Schaffer, and A. Balatsky. “Dirac Materials”. In: *Advances in Physics* 63.1 (Jan. 2, 2014), pp. 1–76. ISSN: 0001-8732. DOI: 10.1080/00018732.2014.927109 (cit. on p. 30).

[55] A. Abouelkomsan, K. Yang, and E. J. Bergholtz. “Quantum Metric Induced Phases in Moir\’e Materials”. In: *Physical Review Research* 5.1 (Feb. 10, 2023), p. L012015. DOI: 10.1103/PhysRevResearch.5.L012015 (cit. on p. 30).

[56] J. Liu and X. Dai. "Orbital Magnetic States in Moiré Graphene Systems". In: *Nature Reviews Physics* 3.5 (May 2021), pp. 367–382. ISSN: 2522-5820. DOI: 10.1038/s42254-021-00297-3 (cit. on p. 30).

[57] N. Witt et al. *Quantum Geometry and Local Moment Swapover in Correlated Graphene Heterostructures*. Mar. 5, 2025. DOI: 10.48550/arXiv.2503.03700. Pre-published (cit. on p. 30).

[58] C. Ghosal et al. *Electronic Correlations in Epitaxial Graphene: Mott States Proximitized to a Relativistic Electron Gas*. Dec. 2, 2024. DOI: 10.48550/arXiv.2412.01329. Pre-published (cit. on p. 30).

[59] K. Momma and F. Izumi. "*VESTA 3* for Three-Dimensional Visualization of Crystal, Volumetric and Morphology Data". In: *Journal of Applied Crystallography* 44.6 (Dec. 1, 2011), pp. 1272–1276. ISSN: 0021-8898. DOI: 10.1107/S0021889811038970 (cit. on p. 31).

[60] W. P. Su, J. R. Schrieffer, and A. J. Heeger. "Soliton Excitations in Polyacetylene". In: *Physical Review B* 22.4 (Aug. 15, 1980), pp. 2099–2111. DOI: 10.1103/PhysRevB.22.2099 (cit. on p. 31).

[61] K. P. Nuckolls and A. Yazdani. "A Microscopic Perspective on Moiré Materials". In: *Nature Reviews Materials* 9.7 (July 2024), pp. 460–480. ISSN: 2058-8437. DOI: 10.1038/s41578-024-00682-1 (cit. on p. 31).

[62] P. A. Pantaleón et al. "Superconductivity and Correlated Phases in Non-Twisted Bilayer and Trilayer Graphene". In: *Nature Reviews Physics* 5.5 (May 2023), pp. 304–315. ISSN: 2522-5820. DOI: 10.1038/s42254-023-00575-2 (cit. on p. 31).

[63] G. Yang et al. "Structure of Graphene and Its Disorders: A Review". In: *Science and Technology of Advanced Materials* 19.1 (Aug. 29, 2018), pp. 613–648. ISSN: 1468-6996. DOI: 10.1080/14686996.2018.1494493 (cit. on p. 31).

[64] D. Jones. *Lattpy*. May 2022. URL: https://github.com/dylanljones/lattpy (cit. on p. 32).

[65] Z.-D. Song and B. A. Bernevig. "Magic-Angle Twisted Bilayer Graphene as a Topological Heavy Fermion Problem". In: *Physical Review Letters* 129.4 (July 19, 2022), p. 047601. ISSN: 0031-9007, 1079-7114. DOI: 10.1103/PhysRevLett.129.047601 (cit. on p. 36).

Not cited

[66] F. Arute et al. “Quantum Supremacy Using a Programmable Superconducting Processor”. In: *Nature* 574.7779 (Oct. 2019), pp. 505–510. ISSN: 1476-4687. DOI: 10.1038/s41586-019-1666-5.

[67] E. Bach. “Parasweep: A Template-Based Utility for Generating, Dispatching, and Post-Processing of Parameter Sweeps”. In: *SoftwareX* 13 (Jan. 1, 2021), p. 100631. ISSN: 2352-7110. DOI: 10.1016/j.softx.2020.100631.

[68] J. G. Bednorz and K. A. Müller. “Possible High Tc Superconductivity in the Ba−La−Cu−O System”. In: *Zeitschrift für Physik B Condensed Matter* 64.2 (June 1, 1986), pp. 189–193. ISSN: 1431-584X. DOI: 10.1007/BF01303701.

[69] A. Beekman, L. Rademaker, and J. van Wezel. “An Introduction to Spontaneous Symmetry Breaking”. In: *SciPost Physics Lecture Notes* (Dec. 4, 2019), p. 011. ISSN: 2590-1990. DOI: 10.21468/SciPostPhysLectNotes.11.

[70] S. M. Chan, B. Grémaud, and G. G. Batrouni. “Pairing and Superconductivity in Quasi-One-Dimensional Flat-Band Systems: Creutz and Sawtooth Lattices”. In: *Physical Review B* 105.2 (Jan. 5, 2022), p. 024502. DOI: 10.1103/PhysRevB.105.024502.

[71] Q. Chen et al. “When Superconductivity Crosses over: From BCS to BEC”. In: *Reviews of Modern Physics* 96.2 (May 23, 2024), p. 025002. DOI: 10.1103/RevModPhys.96.025002.

[72] U. of Chicago. *Annual Register*. 1893-1930., 1896. 462 pp.

[73] L. N. Cooper. “Bound Electron Pairs in a Degenerate Fermi Gas”. In: *Physical Review* 104.4 (Nov. 15, 1956), pp. 1189–1190. DOI: 10.1103/PhysRev.104.1189.

[74] M. I. Faley et al. “High-Tc SQUID Biomagnetometers”. In: *Superconductor Science and Technology* 30.8 (July 2017), p. 083001. ISSN: 0953-2048. DOI: 10.1088/1361-6668/aa73ad.

[75] Y. O. Halchenko et al. “DataLad: Distributed System for Joint Management of Code, Data, and Their Relationship”. In: *Journal of Open Source Software* 6.63 (July 1, 2021), p. 3262. ISSN: 2475-9066. DOI: 10.21105/joss.03262.

[76] C. R. Harris et al. “Array Programming with NumPy”. In: *Nature* 585.7825 (Sept. 2020), pp. 357–362. ISSN: 1476-4687. DOI: 10.1038/s41586-020-2649-2.

[77] T. Hazra, N. Verma, and M. Randeria. "Bounds on the Superconducting Transition Temperature: Applications to Twisted Bilayer Graphene and Cold Atoms". In: *Physical Review X* 9.3 (Sept. 17, 2019), p. 031049. DOI: 10.1103/PhysRevX.9.031049.

[78] H.-L. Huang et al. "Superconducting Quantum Computing: A Review". In: *Science China Information Sciences* 63.8 (July 15, 2020), p. 180501. ISSN: 1869-1919. DOI: 10.1007/s11432-020-2881-9.

[79] K.-E. Huhtinen. "Superconductivity and Normal State Properties in Flat Bands". Aalto University, 2023. URL: https://aaltodoc.aalto.fi/handle/123456789/119970 (visited on 11/27/2024).

[80] J. D. Hunter. "Matplotlib: A 2D Graphics Environment". In: *Computing in Science & Engineering* 9.3 (May 2007), pp. 90–95. ISSN: 1558-366X. DOI: 10.1109/MCSE.2007.55.

[81] K. Irwin and G. Hilton. "Transition-Edge Sensors". In: *Cryogenic Particle Detection*. Ed. by C. Enss. Berlin, Heidelberg: Springer, 2005, pp. 63–150. ISBN: 978-3-540-31478-3. DOI: 10.1007/10933596_3.

[82] B. D. Josephson. "Possible New Effects in Superconductive Tunnelling". In: *Physics Letters* 1.7 (July 1, 1962), pp. 251–253. ISSN: 0031-9163. DOI: 10.1016/0031-9163(62)91369-0.

[83] M. Kang et al. "Measurements of the Quantum Geometric Tensor in Solids". In: *Nature Physics* 21.1 (Jan. 2025), pp. 110–117. ISSN: 1745-2481. DOI: 10.1038/s41567-024-02678-8.

[84] A. M. Klushin et al. "Present and Future of High-Temperature Superconductor Quantum-Based Voltage Standards". In: *IEEE Instrumentation & Measurement Magazine* 23.2 (Apr. 2020), pp. 4–12. ISSN: 1941-0123. DOI: 10.1109/MIM.2020.9062678.

[85] K. Konstantopoulou et al. "Design Optimization and Evaluation of the 3 kA MgB□ Cable at 4.3 K for the Superconducting Link Project at CERN". In: *Supercond. Sci. Technol.* 32.8 (2019), p. 085003. DOI: 10.1088/1361-6668/ab13e7.

[86] S. Linzen et al. "Quantum Detection Meets Archaeology – Magnetic Prospection with SQUIDs, Highly Sensitive and Fast". In: *New Technologies for Archaeology: Multidisciplinary Investigations in Palpa and Nasca, Peru*. Ed. by M. Reindel and G. A. Wagner. Berlin, Heidelberg: Springer, 2009, pp. 71–85. ISBN: 978-3-540-87438-6. DOI: 10.1007/978-3-540-87438-6_5.

[87] W. McKinney. "Data Structures for Statistical Computing in Python". In: Python in Science Conference. Austin, Texas, 2010, pp. 56–61. DOI: 10.25080/Majora-92bf1922-00a.

[88] W. Meissner and R. Ochsenfeld. "Ein neuer Effekt bei Eintritt der Supraleitfähigkeit". In: *Naturwissenschaften* 21.44 (Nov. 1, 1933), pp. 787–788. ISSN: 1432-1904. DOI: 10.1007/BF01504252.

[89] Y. Nakagawa et al. "Gate-Controlled BCS-BEC Crossover in a Two-Dimensional Superconductor". In: *Science* 372.6538 (Apr. 9, 2021), pp. 190–195. DOI: 10.1126/science.abb9860.

[90] K. S. Novoselov et al. "Electric Field Effect in Atomically Thin Carbon Films". In: *Science* 306.5696 (Oct. 22, 2004), pp. 666–669. DOI: 10.1126/science.1102896.

[91] H. K. Onnes. "Further Experiments with Liquid Helium. G. On the Electrical Resistance of Pure Metals, Etc. VI. On the Sudden Change in the Rate at Which the Resistance of Mercury Disappears." In: *Through Measurement to Knowledge: The Selected Papers of Heike Kamerlingh Onnes 1853–1926*. Ed. by K. Gavroglu and Y. Goudaroulis. Dordrecht: Springer Netherlands, 1991, pp. 267–272. ISBN: 978-94-009-2079-8. DOI: 10.1007/978-94-009-2079-8_17.

[92] R. P. S. Penttilä, K.-E. Huhtinen, and P. Törmä. "Flat-Band Ratio and Quantum Metric in the Superconductivity of Modified Lieb Lattices". In: *Communications Physics* 8.1 (Jan. 31, 2025), pp. 1–10. ISSN: 2399-3650. DOI: 10.1038/s42005-025-01964-y.

[93] M. A. Petroff. *Accessible Color Sequences for Data Visualization*. Feb. 29, 2024. DOI: 10.48550/arXiv.2107.02270. Pre-published.

[94] P. A. Rinck. *Magnetic Resonance in Medicine - A Critical Introduction*. ISBN: 978-628-01-2260-1. URL: http://www.magnetic-resonance.org/.

[95] L. Rossi. "Particle Accelerators and Cuprate Superconductors". In: *Physica C: Superconductivity and its Applications* 614 (Nov. 15, 2023), p. 1354360. ISSN: 0921-4534. DOI: 10.1016/j.physc.2023.1354360.

[96] D. Rybicki et al. "Perspective on the Phase Diagram of Cuprate High-Temperature Superconductors". In: *Nature Communications* 7.1 (May 6, 2016), p. 11413. ISSN: 2041-1723. DOI: 10.1038/ncomms11413.

[97] F. Schmidt et al. "Operation Experience and Further Development of a High-Temperature Superconducting Power Cable in the Long Island Power Authority Grid". In: *Physics Procedia*. SUPERCONDUCTIVITY CENTENNIAL Conference 2011 36 (Jan. 1, 2012), pp. 1137–1144. ISSN: 1875-3892. DOI: 10.1016/j.phpro.2012.06.190.

[98] T. pandas development team. *Pandas-Dev/Pandas: Pandas*. Version v2.2.3. Zenodo, Sept. 20, 2024. DOI: 10.5281/ZENODO.3509134.

[99] T. Timusk and B. Statt. "The Pseudogap in High-Temperature Superconductors: An Experimental Survey". In: *Reports on Progress in Physics* 62.1 (Jan. 1999), p. 61. ISSN: 0034-4885. DOI: 10.1088/0034-4885/62/1/002.

[100] A. Tollestrup and E. Todesco. "The Development of Superconducting Magnets for Use in Particle Accelerators: From the Tevatron to the LHC". In: *Reviews of Accelerator Science and Technology* 1.01 (2008), pp. 185–210.

[101] S.-i. Uchida et al. "High Tc Superconductivity of La-Ba-Cu Oxides". In: *Japanese Journal of Applied Physics* 26 (1A Jan. 1, 1987), p. L1. ISSN: 1347-4065. DOI: 10.1143/JJAP.26.L1.

[102] Y. J. Uemura. "Dynamic Superconductivity Responses in Photoexcited Optical Conductivity and Nernst Effect". In: *Physical Review Materials* 3.10 (Oct. 4, 2019), p. 104801. DOI: 10.1103/PhysRevMaterials.3.104801.

[103] United Nations. *International Year of Quantum Science and Technology, 2025*. May 10, 2024. URL: https://docs.un.org/A/78/L.70 (visited on 02/18/2025).

[104] P. Virtanen et al. "SciPy 1.0: Fundamental Algorithms for Scientific Computing in Python". In: *Nature Methods* 17.3 (Mar. 2020), pp. 261–272. ISSN: 1548-7105. DOI: 10.1038/s41592-019-0686-2.

[105] N. Witt. "Electron correlations and unconventional superconductivity in realistic solid state materials and heterostructures". Universität Hamburg.

[106] D. Xiao, M.-C. Chang, and Q. Niu. "Berry Phase Effects on Electronic Properties". In: *Reviews of Modern Physics* 82.3 (July 6, 2010), pp. 1959–2007. DOI: 10.1103/RevModPhys.82.1959.

[107] C. Yao and Y. Ma. "Superconducting Materials: Challenges and Opportunities for Large-Scale Applications". In: *iScience* 24.6 (June 25, 2021), p. 102541. ISSN: 2589-0042. DOI: 10.1016/j.isci.2021.102541.

[108] C. Zhang et al. "Recent Progress on High-Temperature Superconducting Filters". In: *Superconductivity* 2 (June 1, 2022), p. 100012. ISSN: 2772-8307. DOI: 10.1016/j.supcon.2022.100012.

Listings

List of Figures

List of Abbreviations

BCS Bardeen-Cooper-Schrieffer iii, iv, 2, 11, 18

DMFT Dynamical Mean Field Theory iii, iv, 2, 18

BdG Bogoliubov-de Gennes 15, 28

ED Exact Diagonalization 23, 24

FMP Finite Momentum Pairing 29

DFT Density Functional Theory 30

Eidesstattliche Erklärung

Ich versichere, dass ich die Masterarbeit selbstständig angefertigt und keine anderen als die angegebenen Hilfsmittel benutzt habe. Alle Stellen, die dem Wortlaut oder dem Sinn nach anderen Werken entnommen sind, habe ich in jedem einzelnen Fall unter genauer Angabe der Quelle deutlich als Entlehnung kenntlich gemacht. Ich versichere, diese Arbeit nicht bereits in gleicher oder ähnlicher Fassung in einem anderen Prüfungsverfahren eingereicht zu haben.
Sofern im Zuge der Erstellung der vorliegenden Masterarbeit generative Künstliche Intelligenz (gKI) basierte elektronische Hilfsmittel verwendet wurden, versichere ich, dass meine eigene Leistung im Vordergrund stand und dass eine vollständige Dokumentation aller verwendeten Hilfsmittel gemäß der Guten wissenschaftlichen Praxis vorliegt. Ich trage die Verantwortung für eventuell durch die gKI generierte fehlerhafte oder verzerrte Inhalte, fehlerhafte Referenzen, Verstöße gegen das Datenschutz- und Urheberrecht oder Plagiate.
Ich bin damit einverstanden, dass die Masterarbeit veröffentlicht wird.

Statutory Declaration

I declare that I have authored the Master's thesis independently and have not used any aids other than those specified. I have clearly labelled all passages that are taken from other works in terms of wording or meaning as borrowed material, stating the exact source in each case. I confirm that I have not already submitted this thesis in the same or a similar version in another examination procedure.
If electronic aids based on generative artificial intelligence (gAI) were used in the course of the preparation of this Master's thesis, I confirm that my own work was the main focus and that complete documentation of all aids used is available in accordance with good scientific practice. I am responsible for any incorrect or distorted content, incorrect references, violations of data protection and copyright law or plagiarism generated by the gAI.
I agree that the Master's thesis may be published.

Ort, Datum	Unterschrift